國立台灣師範大學理學院地球科學系所
碩士論文
Department of Earth Sciences
College of Science
National Taiwan Normal University
Master Thesis

紅外線明亮星系的活躍星系核特性
The Role of AGNs in the (Ultra)Luminous Infrared Galaxy

指導老師： 橋本康弘 教授 & 傅谷石 教授
Supervisors:
Prof. Yasuhiro Hashimoto & Prof. Sébastien Foucaud
研究生：林明儀
Student: Ming-Yi Lin

中華民國 102 年 7 月
July, 2013

Contents

Tables

Figures

ABSTRACT

In order to understand the mutual influence between active galactic nuclei (AGN) and star formation during the evolution of galaxies, we investigate 142 galaxies detected in both X-ray and 70μm observations in the COSMOS (Cosmic Evolution Survey) field. All of our data are obtained from archive, X-ray point source catalogs from Chandra and XMM-Newton observation; far-infrared 70μm point source catalog from Spitzer-MIPS observation. Although the IRAC [3.6μm]-[4.5μm] vs. [5.8μm]-[8.0μm] colors of our sample indicate the existence of star formation, the ratio of rest frame 2-10 keV luminosity to total infrared luminosity (8-1000μm) shows comparatively higher X-ray flux than submillimeter galaxies for a given total infrared luminosity, indicating the possibility of higher AGN activity relative to star formation. When we characterize "obscured AGN" by X-ray hardness ratio, we find that sources with exhibit both 70μm and X-ray emissions tend to have a higher hardness ratio compared to X-ray sources without 70μm emission, suggesting possible connection between the dust and gas across the various physical scales inside a galaxy. We also find that 70μm detected galaxies with X-ray emission and without X-ray emission show no significant difference in cold dust temperature, suggesting that the AGN activity and the dust temperature may not be directly correlated.

Subject headings: high-redshift – galaxies: active – infrared: galaxies – X-rays: galaxies.

1. INTRODUCTION

Both observational and simulation evidences over the past decades strongly suggest the existence of supermassive black hole (SMBH) within the spherical bulge of galaxies. The tight connection between the SMBH mass and the bulge properties, such as bulge luminosity or stellar velocity dispersion, indicates a scenario of co-evolution for central black hole and its host galaxy (Kormendy & Richstone 1995; Magorrian et al. 1998). Galaxy merger is a plausible interpretation to explain the concomitant growth of black hole and host galaxy under the ΛCDM model (Treister et al. 2010). Such interpretation suggests the mergers distort galaxy morphology, reducing angular momentum that induces gas accumulation around circumnuclear region easily (Barnes & Hernquist 1991). During the starburst epoch, a large amount of dust and molecular gas around central region (Chung et al. 2011; Magdis et al. 2011) can be interpreted as remnants of supernova explosions and stellar wind from evolved stars. For instance, the local infrared luminous galaxy Arp 220 has been confirmed higher supernova rate from radio observation that supports star formation drives its enormous infrared luminosity (Lonsdale et al. 2006a). Meanwhile, interstellar medium (ISM) is also funneled onto the SMBH in the galactic nucleus and consequently triggers a phase of active galactic nuclei (AGNs), with its powerful electromagnetic radiation spanning from radio to gamma-ray. In the later galaxy evolution stage, the merger scenario suggests that the radiation-pressure or kinematic-wind feedback from AGN may quench the star formation, disrupting the remnant gas and dust. At the same time, central AGN turns into an optically unobscured quasar, a class of luminous AGN. Final outcome in galaxy evolution is a red elliptical galaxy (Hopkins et al. 2008, and references therein).

Sanders et al. (1988a) first proposed a connection between the Ultra Luminous Infrared Galaxies (ULIRGs; $L_{\rm IR} \geq 10^{12} L_{\odot}$) and quasars as two successive snapshots of merger event between two gas-rich spiral galaxies. Indeed, from IRAS 1 Jy ULIRGs studies, the merger-ULIRG connection has been revealed by a large fraction of interacting galaxies at $z < 0.1$ (Borne et al. 2000; Cui et al. 2001; Veilleux et al. 2002). Besides, the merger fraction has been shown to increase as infrared luminosity raises, merging galaxy being prevalent population amongst ULIRGs to redshift ~ 1 (Shi et al. 2009). However at higher redshift ~ 2, the merging galaxy fraction drops slightly and non-interacting disk galaxy fraction increases (Kartaltepe et al. 2012).

On the other hand, the merger-AGN connection is more difficult to observe. Although, in the local universe, optical luminous quasars are considered to be related to post-starburst merger stage (Canalizo & Stockton 2001; Bennert et al. 2008), at $1.5 < \mathrm{z} < 2.5$, AGNs are more likely to occur inside of normal disk or bulge galaxy, instead of interacting systems, suggesting that secular processes (such as bars or nucleus rings) may trigger nuclear activity instead of major-mergers (Schawinski et al. 2011; Kocevski et al. 2012). The connection between ULIRGs and AGNs has been investigated for the past few years. The AGN fraction seems to rise with the infrared luminosity increased (Genzel & Cesarsky 2000; Kartaltepe et al. 2010). The AGN activities couple with their infrared spectral energy distribution (SED) profile, the higher mid-infrared color ratio (i.e. $F25/F60 \geq 0.2$), which classified as warm ULIRGs, is believed to dominate by AGN. Otherwise, lower mid-infrared color ratio (i.e. $F25/F60 \leq 0.2$) is classified as cold ULIRGs, dominating by star formation (Sanders et al. 1988b; Veilleux et al. 2009).

In order to determine the exact role of the AGN in the overall galaxy evolution, it is essential to separate the AGN contribution from the normal star formation activity. To decouple two components, three distinct methods can be used:
(i) *Specific emission lines ratio* - Fine structure radiation in optical and infrared wavelength are reliable tracers of excitation state of the ISM in galaxies. A classification based on two independent line ratios can help to segregate AGN and star-forming galaxies. For

instance, investigating [OIII]5007Å/Hβ versus [NII]6584Å/Hα (Baldwin et al. 1981, BPT) diagram will lead to distinguish the photoionization, derived from normal HII regions, from power-law continuum generated by AGNs. Unfortunately, galaxies undergoing merger event suffer from dust obscuration in optical wavelength that limits the efficiency of such diagnostics, but not likely misclassify the AGN identification (Veilleux 2002; LaMassa et al. 2012).

By the advent of the infrared spectrometer on the Infrared Space Observatory (ISO) and the Spitzer telescope, additional emission lines were identified for AGN diagnostics in the mid-infrared that are less sensitive to extinction. For example, the line ratio [O IV]25.9μm/[Nell]12.8μm or [NeV]14.3μm/[Nell]12.8μm is a reliable indicator to separate AGNs from star-forming galaxies (Genzel et al. 1998; Armus 2006). The different transition lines of 6.2μm 7.7μm and 11.3 μm Polycyclic Aromatic Hydrocarbon (PAH) molecules are other reliable star formation tracers, with weaker PAH emission corresponds to higher AGN contribution.(Voit 1992; Veilleux et al. 2009);

(ii) *Continuum slope* - In contrast with cold dust components in far-infrared are powered by star formation, hot dust components around 10μm are considered to be associated with AGN influence. As the influence of the AGN becomes significant in the galaxy, the infrared spectral indexes start to be dominated by a power-law continuum $\sim$ 10μm (Alonso-Herrero et al. 2006; Donley et al. 2007). Therefore, the mid-infrared to far-infrared ratio is a simple measure to quantify the relative contributions of AGNs and star-forming galaxies (Veilleux et al. 2009);

(iii) *Spectral energy distribution fitting* - With the development of deep multi-wavelength photometric surveys, panchromatic Spectral Energy Distribution (SED) studies are becoming increasingly popular. Theoretical or empirical templates are commonly used to fit the SED and determine the photometric redshifts of galaxies. Multi-component fitting, including the contribution from stars, dust, and AGNs is now possible thanks to very broad photometric coverage. In the case of heavily obscured AGNs, although star formation of host galaxy dominates the flux at most wavelengths, a bump in mid-infrared produced by the circumnuclear dust radiation, can be an indicator of an obscured AGN. Therefore, identifying hot dust component from the galaxy SED is a reliable way to determine the AGN contribution to total infrared luminosity (Mullaney et al. 2011; Pozzi et al. 2012).

Although the different methods may not agree completely on defining a pure sample (i.e. pure-AGN or pure starburst galaxy), they all provide evidences that, for the major part of the samples, AGN and star formation occur concomitantly. Except pursuing the intrinsic AGN contribution fraction on the total infrared luminosity, what is essential here is to understand the mutual influence on the properties of AGNs and hosts star-forming galaxies. We tried to investigate whether the dust from star formation in host galaxy could obscure central AGN and the presence of AGN radiation could change the far-infrared SED.

The SEDs of Luminous Infrared Galaxies (LIRGs; $10^{11}L_{\odot} \leq L_{\rm IR} < 10^{12}L_{\odot}$) and ULIRGs are peaked in the range of 40-200μm (Sanders & Mirabel 1996). In fact, the 70μm Spitzer band is ideal to unambiguously trace star-forming galaxies as it is little affected by PAH emissions, silicate absorption, and stellar flux. Central AGNs are usually identified by their strong X-ray continuum emission. Indeed, high energy X-ray photons emitted by hot corona of accretion disk (e.g., Haardt & Maraschi 1993) around the central black-hole are usually little absorbed by dust and gas from host galaxies, compared to lower energy UV-photons. One noticeable exception are compton thick objects ($N_H \geq 10^{24}$ cm^{-2}) for which even hard X-ray photons are absorbed. Compton thick AGNs are not uncommon existence among ULIRG population. In local universe, Lonsdale et al. (2006b) have concluded that the presence of Fe Kα lines and flat spectrum in ULIRGs indicate the Compton-thick AGN harbors inside the central region (e.g. Mrk 273 in Balestra et al. (2005) paper). In higher redshift, although different Compton-thick candidate selections (e.g.

24μm excess, mid-infrared spectral slope, and radio excess) are not complete coincidence (Bauer et al. 2010), the Compton-thick fraction is significantly increased in early universe (Brightman & Ueda 2012).

Several studies have investigated the nature of the 70μm galaxy population. Patel et al. (2011) lead a spectroscopic follow-up in optical wavelength of 70μm galaxies selected from the Spitzer Wide-area Infrared Extragalactic Legacy Survey. Their results suggest that the most of the IR photons are powered by star formation, while contribution from AGN dusty torus emission are negligible for the non-QSO-dominated samples. From the SED study of 61 out of 70μm selected galaxies from the 0.5 deg^2 wide Extended Groth Strip (EGS) field, Symeonidis et al. (2010) concluded that, even in the presence of powerful hard X-ray emission originated from AGNs, dust emission components are required to explain the observed strong far-infrared luminosity. To reveal a potential starburst-AGN connection, Trichas et al. (2009) used 28 X-ray sources with 70μm detection galaxies and applied a statistical K-S test (Kolmogorov-Smirnov test) to assess divergency in hardness ratio between X-ray detected 70μm galaxies and the whole X-ray population in the redshift interval 0.5 $<$ z $<$1.5. However, the hardness ratio result leads to a less significant probability of the K-S test, in contrast to current co-evolution of AGN and host galaxy that the central region is obscured by dust and gas due to circumnuclear starburst (Hopkins et al. 2008).

In this paper, we aim to dissect the role of AGN in the infrared (ultra)luminous phase of galaxy evolution. We extracted the X-ray detected sub-sample from unconfused 70μm catalog. Our main 70μm galaxy catalog was published by Kartaltepe et al. (2010), including total infrared luminosity, multi-wavelength photometry and redshift. We describe the data used for this work in section 2. As we are interested in physical property of AGN and far-infrared selected host galaxy, we cross-match X-ray and 70μm datasets. In section 3, we depict our matching method as well as the methods used to estimate and calibrate different physical parameter measurements. We present our results in section 4, and then conduct a detailed discussions in section 5. Throughout this paper, we adopt a fiducial cosmological model with the following parameters: $H_0 = 70$ km s^{-1} Mpc^{-1}, and $\Omega_M = 0.3$, $\Omega_\Lambda = 0.7$. Unless otherwise stated, all magnitudes in this paper are in the Vega system.

2. DATA

The Cosmic Evolution Survey (COSMOS) is the largest treasury program using Hubble Space Telescope, imaging a $\sim$2 deg^2-wide equatorial field in the optical F814W filter (approximately corresponds to I band) with the Advanced Camera for Surveys (ACS) instrument (Scoville et al. 2007a,b; Koekemoer et al. 2007). Several large follow-up campaigns using ground-based and space-based telescopes produced the deepest comprehensive photometric and spectroscopic dataset across a whole spectrum (Capak et al. 2007; Hasinger et al. 2007; Sanders et al. 2007; Scott et al. 2008)[1]. Our initial catalog is a 70μm catalog extracted by Kartaltepe et al. (2010), who have publicly released their measured total infrared luminosity, redshifts, and multi-wavelength photometry. Here, we will give a brief description of our infrared and X-ray datasets.

2.1. Spitzer-COSMOS

Spitzer-COSMOS (S-COSMOS) is a Legacy program designed to cover the COSMOS field with deep Spitzer observations in IRAC four bands (i.e. 3.6, 4.5, 5.8, and 8.0μm) and MIPS three bands (i.e. 24, 70, and 160μm). The initial Cycle 2 program conducted in 2006

[1] c.f. the COSMOS Special Issue of the Astrophysical Journal Supplement Series, in September, 2007.

consists of a deep IRAC survey and a narrow-field MIPS survey. The total integration time of the deep IRAC survey is 166 hours, reaching 5σ sensitivities of 0.9, 1.7, 11.3, and 14.6 μJy, in 3.6, 4.5, 5.8, and 8.0μm band, respectively (Sanders et al. 2007). A complementary MIPS deep observation of 450 hours has been conducted in Cycle 3, ensuring accurate 70 and 160μm flux density measurements. The median exposure times were $\sim$ 3400s, 1350s, and 270s for 24μm, 70μm, and 160μm band, respectively, corresponding to 5σ depths of $\sim$ 0.08, 8.5, and 65 mJy (Le Floc'h et al. 2009; Frayer et al. 2009; Kartaltepe et al. 2010).

2.2. X-ray dataset: XMM-Newton & Chandra

The COSMOS field has been covered with observation from both XMM-Newton (XMM) and Chandra observatories.

A 2 deg^2 contiguous survey has been conducted with XMM to reach medium depth ($\sim$60 ks). COSMOS X-ray catalog made by XMM observation (XMM-COSMOS) provides three different energy bands. Base on the logN-logS relationship, the flux limit of 0.5-2 keV (soft band), 2-10 keV (hard band), and 5-10 keV (ultra-hard band) drop to 7.2 x 10^{-16} ergs cm^{-2} s^{-1}, 4.0 x 10^{-15} ergs cm^{-2} s^{-1}, and 9.7 x 10^{-15} ergs cm^{-2} s^{-1}, respectively (Hasinger et al. 2007; Cappelluti et al. 2009). In total, 1887 point-like sources were identified in the XMM-COSMOS survey. Brusa et al. (2010) has released a cross matched catalog between these sources and optical counterparts (I band, catalog of Capak et al. (2007)), providing redshifts (spectroscopic and photometric), UV to 24μm photometry, and hardness ratio.

The Chandra-COSMOS (C-COSMOS) Survey images a $\sim$0.9 deg^2 field in the central part of the original COSMOS field, with the effective exposure time $\sim$160 ks in center 0.5 deg^2 and $\sim$80 ks in outer 0.4 deg^2. C-COSMOS catalog provides three different energy bands, 0.5-2 keV (soft band), 2-7 keV (hard band), and 0.5-7 keV (full band), with corresponding flux limits of 1.9 x 10^{-16} ergs cm^{-2} s^{-1}, 7.3 x 10^{-16} ergs cm^{-2} s^{-1}, and 5.7 x 10^{-16} ergs cm^{-2} s^{-1}, respectively. In total, 1761 point-like sources have been extracted in the in C-COSMOS field (Elvis et al. 2009).

In this paper, we combine observations from XMM and Chandra, taking advantage of the wider observational field of XMM-COSMOS and the deeper observational depth of C-COSMOS, to maximize the total number of X-ray point source counterparts of our 70μm selected galaxy sample.

3. METHOD

3.1. Matched X-ray and far-infrared point source catalog

The spatial resolution of the Spitzer Telescope at 70μm is around 18$''$, much larger than the spatial resolution of XMM or Chandra X-ray observatory. Therefore, it is crucial to accurately detect the position of the 70μm galaxies. Kartaltepe et al. (2010) have identified 1503 optical or near-IR counterpart of 70μm selected galaxies (refer to Kartaltepe et al. (2010) in Section 3.1). We took advantage of the Altas resource from IRSA/COSMOS archive [2] to match the optically or near-IR identified counterpart of 70μm selected sources with the XMM and Chandra point source catalogs, separately. We identified 108 and 92 out of 70μm counterparts by matching with XMM and Chandra, using searching radii of 3" and 1" separately. The median angular distances between the position of the X-ray source and the position of optical/near-IR identified counterpart of our 70μm-selected galaxies are 0.9$''$ and 0.3$''$ for the XMM and Chandra point source catalogs, respectively. Fifty-eight sources were identified in both X-ray catalogs, and a total number of one hundred and forty-two galaxies have been identified to have both 70μm and X-ray measurements in the COSMOS

[2]NASA/IPAC infrared service archive of COSMOS project. http://irsa.ipac.caltech.edu/data/COSMOS

Table 1: Samples properties and matching results

Catalog	Area [a] in deg^2	Flux limits [b] in mJy (†) or 10^{-16}ergs cm^{-2} s^{-1} (‡)		N_S [c]	$N_{70\mu m}$ [d]	References [e]
Spitzer-COSMOS (S-COSMOS) 70μm galaxies catalog	2.47	8.5 (†)	(5σ)	1503	1503	Frayer et al. (2009) & Kartaltepe et al. (2010)
XMM-COSMOS Point source catalog	2.13	7.2 (‡)	(Soft band)	1886	108	Cappelluti et al. (2009) & Brusa et al. (2010)
		40 (‡)	(Hard band)			
		97 (‡)	(Full band)			
Chandra-COSMOS (C-COSMOS) Point source catalog	0.50(Deep)	1.9 (‡)	(Soft band)	1761	92	Elvis et al. (2009)
	0.40(Shallow)	7.3 (‡)	(Hard band)			
		5.7 (‡)	(Full band)			
XMM- & Chandra-COSMOS concatenated catalog [f]	–	–		2821	142	This work

[a]Effective area covered by the survey; [b] Flux limit of the catalog; [c]Total number of sources; [d]Number of sources cross-matched with the 70μm catalog; [e]References describing the catalog; [f]Catalog concatenated from XMM- and Chandra-catalogs; sources matched between the two catalogs are not duplicated; the cross-match between this catalog and the 70μm catalog constitute our primary "70μm/X-ray " catalog.

field. We will refer to this sample as "70μm/X-ray " galaxy catalog in the remaining part of this article. From the same datasets, Kartaltepe et al. (2010) identified 154 X-ray detected 70μm galaxies (refer to Figure 7 in their paper). The 12 extra objects compared to our own matching catalog are originated from a slightly less strict matching criterion. We speculated these additional sources are more distant from the 70μm source position. The number of sources from our different catalogs and matched catalogs are summarized in Table 1.

3.2. Redshift determination

We extracted the redshift information from Kartaltepe et al. (2010) catalog. Their catalog includes spectroscopic redshift and photometric redshift, we will introduce the detail in following paragraph.

Several spectroscopic surveys were conducted to measure the redshifts of galaxies in the COSMOS field. The most extensive survey on this field is the zCOSMOS survey (Lilly et al. 2007), a deep spectroscopic survey conducted with the VLT-VIMOS multi-object spectrograph to study the evolution of faint/obscured galaxies through direct analysis of their emission lines. Although the observations enable us to probe properties of faint objects, only the central 1 deg^2 is covered by zCOSMOS. Forty-nine of our 70μm/X-ray galaxies had their redshifts confirmed spectroscopically by zCOSMOS. Observations using other facilities have been conducted on this field providing precise redshifts for fifty-three additional 70μm/X-ray galaxies (Abazajian et al. 2009; Trump et al. 2007; Kartaltepe et al. 2010; Prescott et al. 2006). In total 102/142 (72%) galaxies with X-ray and 70μm detection have spectroscopic redshift. Table 2 summarize the origin and number of our targets with spectroscopic redshifts.

For the remaining galaxies, we used the photometric redshift catalogs built for both non-AGN sources and XMM-selected sources (Ilbert et al. 2009; Salvato et al. 2009), using the public available software Le PHARE[3] (Arnouts et al. 1999; Ilbert et al. 2006). The 70μm/X-ray galaxies which do not have spectroscopic redshift have been assigned a photometric redshift (40 out of 142 - 28%).

The photometric and spectroscopic redshifts of 70μm/X-ray galaxies follow the overall 70μm galaxy relation with a scatter of $0.02 \times (1+z)$ (Kartaltepe et al. 2010). Bright sources have usually been assigned a spectroscopic redshift, with small error, while faint sources have been assigned a photometric redshift with larger error. Fortunately, even though these two different methods for redshift measurement have different error sizes, the infrared and X-ray luminosity distribution inferred both by spectroscopically and photometrically determined redshfits have the same median value. Therefore, we conclude the difference in redshift measurements does not induce any systematic bias.

3.3. Total infrared luminosity

Kartaltepe et al. (2010) estimated the total infrared luminosity ($L_{\rm IR}$) for all 70μm-selected galaxies, by fitting a SED with a χ^2-minimization method using *Le PHARE*[3] and integrating the luminosity over the 8-1000μm wavelength range.

The current public COSMOS 70μm-catalog from Kartaltepe et al. (2010) has been constructed carefully taking into account the possible AGN contamination: they only used 24, 70, and 160 μm photometric data. However, this catalog suffers incompleteness in the 160μm band, and lacks any direct photometric observation in Rayleigh-Jeans part of the SED. Kartaltepe et al. (2010) assessed that measurements of $L_{\rm IR}$ without 160μm data are underestimated by 0.2 dex compared to measurements with 160μm data. Despite

[3]http://www.cfht.hawaii.edu/~arnouts/LEPHARE

these caveats, we estimate that this catalog is robust enough for our study, as the galaxies without 160μm photometry are equally spread between the samples with or without X-ray detected 70μm galaxies.

We divided our 70μm/X-ray galaxy sample into three distinct classes according to their total infrared luminosity as star-forming galaxy (SFG), luminous infrared galaxy (LIRG), and ultra-luminous infrared galaxy (ULIRG) with $L_{\rm IR} < 10^{11}L_{\odot}$, $10^{11}L_{\odot} \leq L_{\rm IR} < 10^{12}L_{\odot}$, and $L_{\rm IR} \geq 10^{12}L_{\odot}$, respectively. Figure 1 shows the redshift distribution in different infrared luminosity intervals, SFGs with median $z \sim 0.168$, LIRGs with median $z \sim 0.518$, and ULIRGs with median $z \sim 1.268$.

3.4. Estimating dust temperature of host galaxy

In the local universe, the far-infrared luminosity is assumed to be driven by the emission from dust grains contained in the galaxy. Far-infrared photometry becomes a critical indicator to reveal the dust properties of the galaxy. Owing to the deep Spitzer observations, we identified 463 far-infrared 160 μm counterparts out of 70μm sources (463 out of 1503; 31%), amongst which 52 (52 out of 142; 37%) counterparts are defined as 70μm/X-ray galaxies. Most (89%, $\sim$ 417/463) of 160μm detected sources have a single matched 70μm source inside MIPS error circle. While for the remaining sources with multiple 70μm counterparts, Kartaltepe et al. (2010) assigned the brighter one as counterpart of the 160μm source.

Using the 70μm and 160μm fluxes, we adjusted a single temperature model represented by a modified blackbody radiation, as following:

$$F_{\nu} = \nu^{\beta} B_{\nu}(\nu, T) \tag{1}$$

with a fixed emissivity $\beta \sim 1.5$ (Clements et al. 2010)

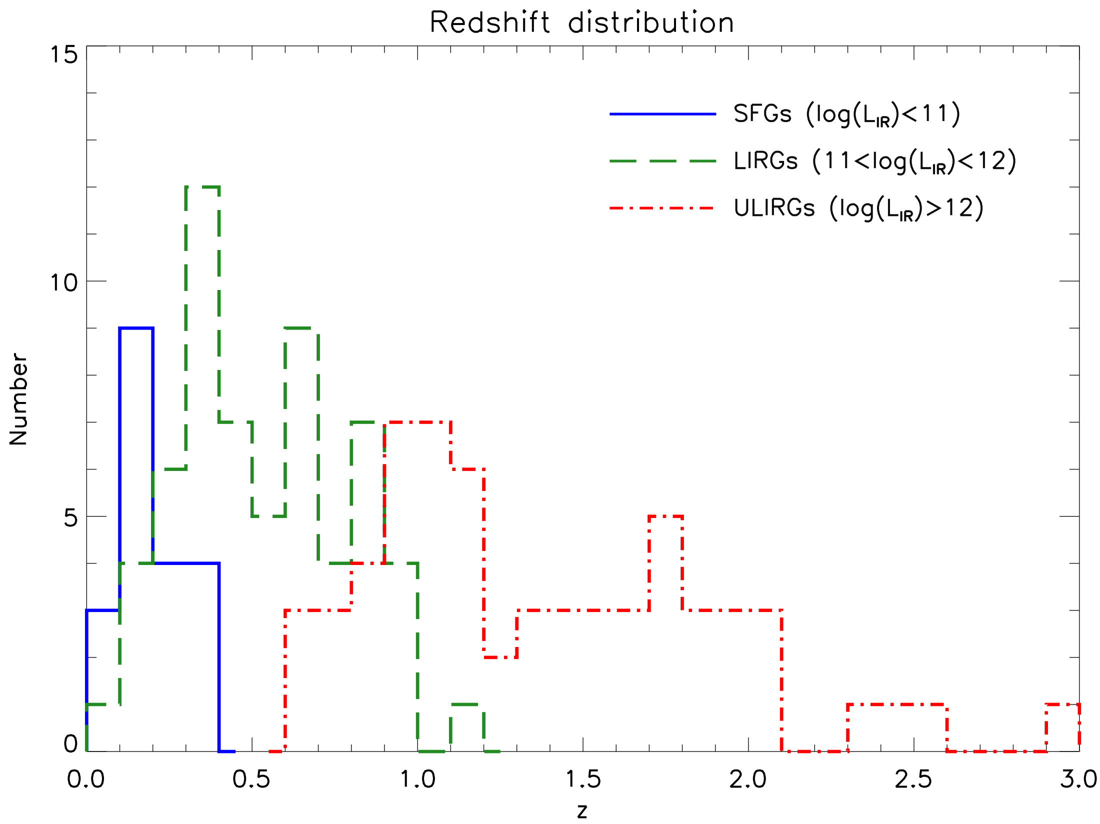

Fig. 1.— The redshift distribution of 70μm/X-ray galaxies. We divided our total sample into three distinct classes selected according to their total infrared luminosity : star-forming galaxies (SFGs; $L_{\rm IR} < 10^{11} L_\odot$; blue solid line) at a median redshift of $z \sim 0.168$, luminous infrared galaxies (LIRGs; $10^{11} L_\odot \leq L_{\rm IR} < 10^{12} L_\odot$; green dash line) at $z \sim 0.518$ and ultra-luminous infrared galaxies (ULIRG; $L_{\rm IR} \geq 10^{12} L_\odot$; red dash-dot line) at $z \sim 1.268$.

We restrict the temperature as free parameter, ranges from 5K to 205K, typical dust temperature for submillimeter galaxies (SMGs) and ULIRG (Chapman et al. 2005; Kovács et al. 2006; Yang et al. 2007; Casey et al. 2009). Models are convolved with Spitzer-MIPS filter response, and the best temperature is fitted using a minimum χ^2 method:

$$\chi^2 = \sum_i [\frac{F_{obs,i} - nF_{model,i}}{\sigma_i}]^2 \tag{2}$$

where i refers to 70μm and 160μm flux densities and n is the normalization factor to the 160μm flux density. We have normalized the model 160μm flux density to observed 160μm flux density because far-infrared could truly represent the cold dust temperature continuum. In order to simulate the observed flux from our assumed temperature models, we also have applied the absolute calibration, color correction factors of 0.918 and 0.959 for the 70μm and 160μm bands, respectively (Stansberry et al. 2007; Frayer et al. 2009). The 90% of χ^2 fitting results are below 0.00125.

To ensure an accurate estimation of the dust temperature in high-redshift galaxies, we exclude the 24μm fluxes from our SED fitting, mainly because of:
(i) Contamination of the flux in the 5-30μm range by emissions from the AGN dust torus or alternatively a potential hot dust component (Brand et al. 2006; Pozzi et al. 2012),
(ii) Presence of several Polycyclic Aromatic Hydrocarbon (PAH) transition lines (e.g. 6.2, 7.7, and 11.3μm emission lines) entering the 24μm band at z$\sim$1, (iii) Presence of strong silicate absorption feature at 9.7μm, which is strongly correlated with the optical depth; in particular in the case of ULIRGs, presence of large amount of dust grains causes the distinct absorption features (Levenson et al. 2007).

3.5. Correction of X-ray properties

With the help of combining both XMM and Chandra X-ray catalogs, we extend our total sample of 70μm/X-ray galaxies to 142 sources, of which 58 are listed in both X-ray catalogs. The count rates for these sources have been converted into $0.5-2$keV (soft band) and $2-10$keV (hard band) flux for both XMM and Chandra observations by assuming different power-law indices. Indeed, XMM and Chandra used 2-8 keV and 2-7 keV energy band for collecting hard X-ray counts. In order to estimate the hard band flux (e.g. 2-10 keV) from count rates, XMM and Chandra observations assumed $\Gamma \sim 1.7$ and 1.4, respectively (Cappelluti et al. 2009; Elvis et al. 2009). For the 58 sources with overlapping detections between the two catalogs, we confirmed both hard and soft band flux from XMM and Chandra are consistent. The correlation in soft band follows the 1:0.9 relation with 1 σ dispersion of 0.063 in log scale, the correlation in hard band follows the 1:1.1 relation with 1 σ dispersion of 0.034 in log scale. Figure 2 show the correlation of hard X-ray luminosity between XMM and Chandra observations.

Given the large redshift range covered by our sample (see Figure 1), it is necessary to apply k-corrections to compute the X-ray rest-frame luminosities of our 70μm/X-ray galaxy sample. We assumed that the spectrum of our galaxies in X-ray follows a simple power law with photon index $\Gamma = 1.7$, and derived the ratio between rest-frame and observe-frame flux integration, to compute the rest-frame flux. Although the different Γ assumption would affect k-correction factor, the luminosity of hard X-ray does not have significant change, we still applied $\Gamma = 1.7$ for 70μm/X-ray galaxy sample whether they extracted from Chandra catalog or not.

One of the main goals of our study is to explore the relationship between the galaxy host extinction and the central region obscuration. However, the neutral hydrogen column density identified in X-ray is integrated on the line-of-sight, therefore estimations of the

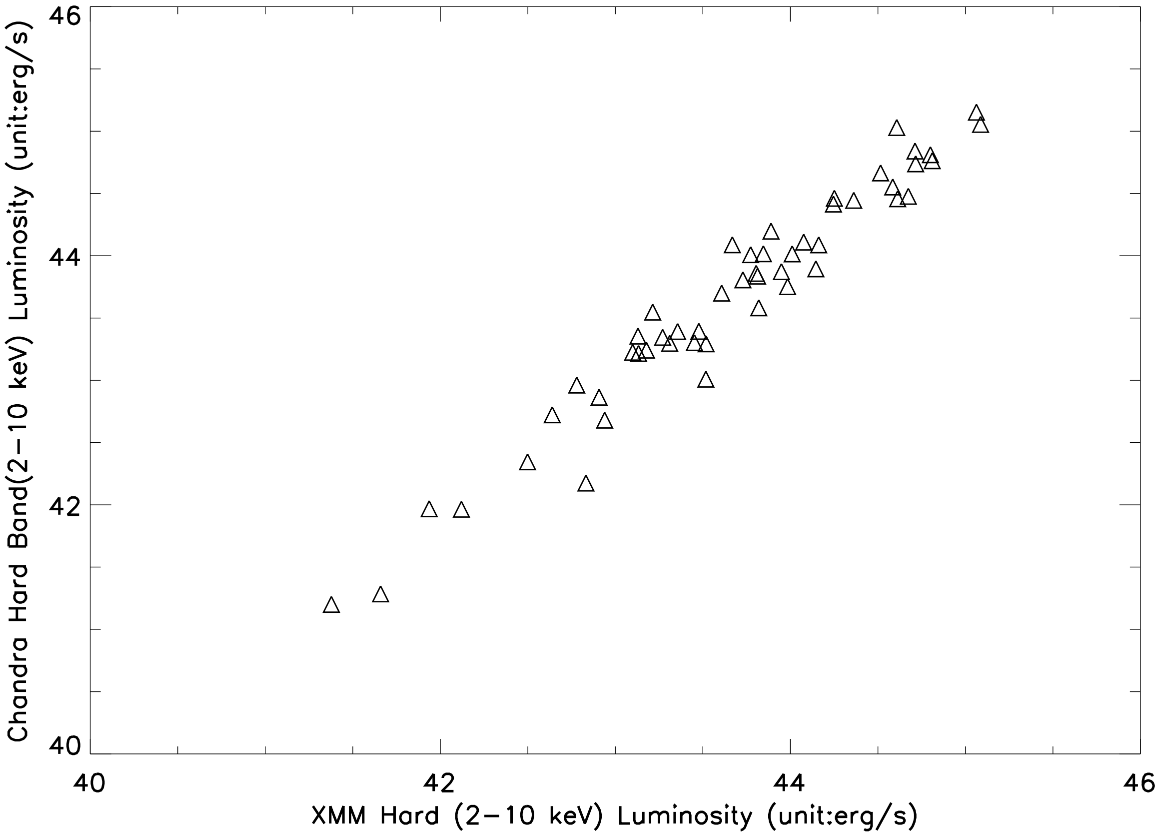

Fig. 2.— Hard X-ray luminosity from the Chandra catalog (Elvis et al. 2009) versus hard X-ray luminosity from the XMM catalog (Brusa et al. 2010) for our 70μm/X-ray galaxies. The correlation factor follows a well-fit 1:1.1 relation with 1 σ dispersion of 0.034 in log scale.

intrinsic column density from X-ray spectrum fitting become model-dependent (Akylas et al. 2006). In order to simplify our analysis, we decided to use the hardness ratio (hereafter HR) as a good proxy of central region obscuration, define as:

$$HR = \frac{H - S}{H + S} \tag{3}$$

where H is X-ray hard band counts and S is X-ray soft band counts.

Our HR values are extracted from Brusa et al. (2010) for XMM observations and Elvis et al. (2009) for Chandra observations. To calibrate our empirical conversion factor, we take advantage of our sources detected in both observatories. In Figure 3, we compared the HR from XMM with the HR from Chandra, for the overlapping detected sources. We have employed a linear fitting for 38 of 70μm/X-ray galaxies, which have both HR from XMM and Chandra. The result followed a 1.03:1 correlation with 1 σ dispersion $\sim$ 0.06 ($\chi^2 \sim 0.4$). The spectral variability could induce the inconsistency in different observations, Mateos et al. (2007) have summarized the Δ $\Gamma \sim 0.2$ changes in observed X-ray color of Δ HR $\sim$ 0.1. In fact, our typical HR dispersion is $\sim$ 0.05 - 0.1, it cannot rule out the influence of spectral variability among our samples. Flux variable AGNs are another uncertainty, HR suffers the flux variability that will hard to derived the value of absorption accurately. According to former paragraph, the hard and soft band luminosity from XMM and Chandra are almost keeping the consistency that we could conclude there is less contribution in our samples from flux variation. In order to unify HRs from different observations, all of our HR values are in XMM band system.

There is 96/142 (68%) of the 70μm/X-ray sources are detected in both soft and hard X-ray band that provided the well-defined HR values. For the rest 46/142(32%) objects, 24 are only soft band detection, 21 are only hard band detection, and 1 is full band detection (neither detected in soft band nor hard band). For the purpose of presenting intrinsic hard X-ray luminosity, correcting the absorption by neutral hydrogen is obligatory. We

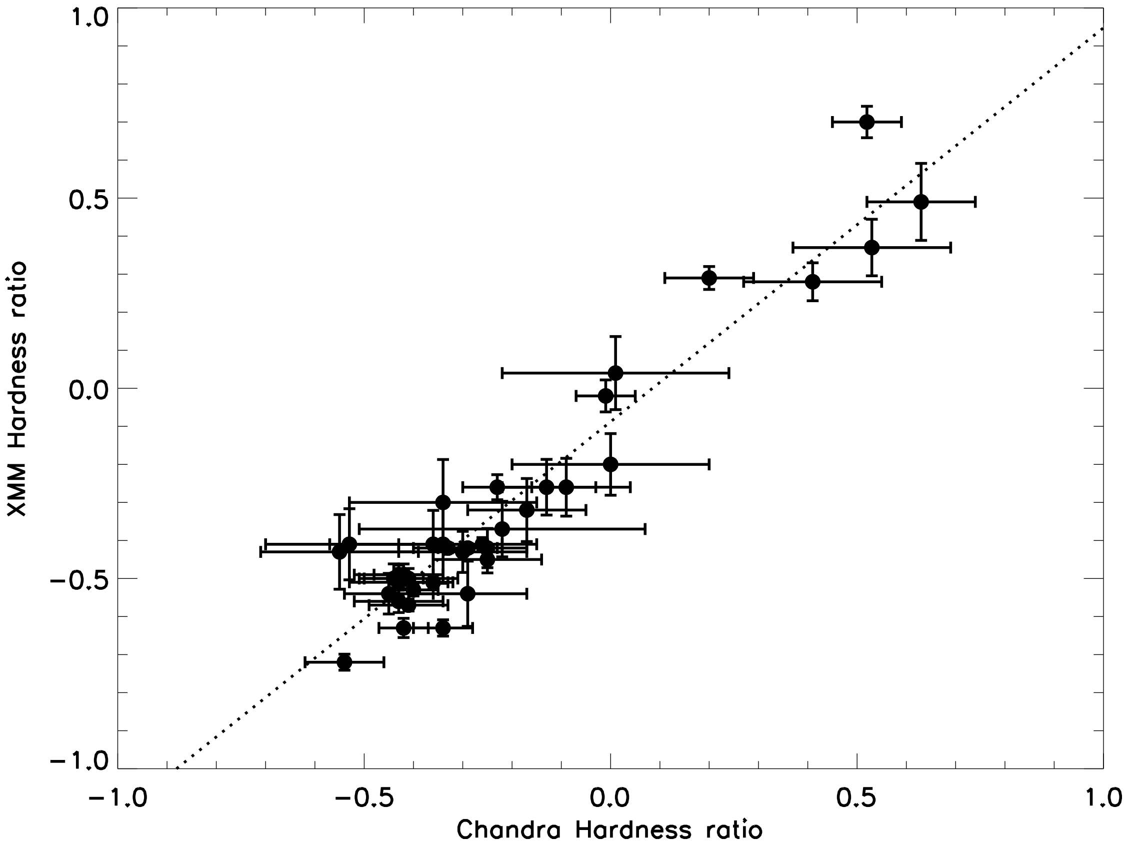

Fig. 3.— Hardness ratio extracted from the XMM catalog (Brusa et al. 2010) vs. value from the Chandra catalog (Elvis et al. 2009) for our 38 sources detected with both observatories. The different hard X-ray energy bands between the two observations, influence the hardness ratio measurements. We fit a simple line to estimate a conversion factor between the two different measurements. The fitted conversion factor is of 1.03 with small dispersion 1 $\sigma \sim 0.06$ ($\chi^2 \sim 0.4$).

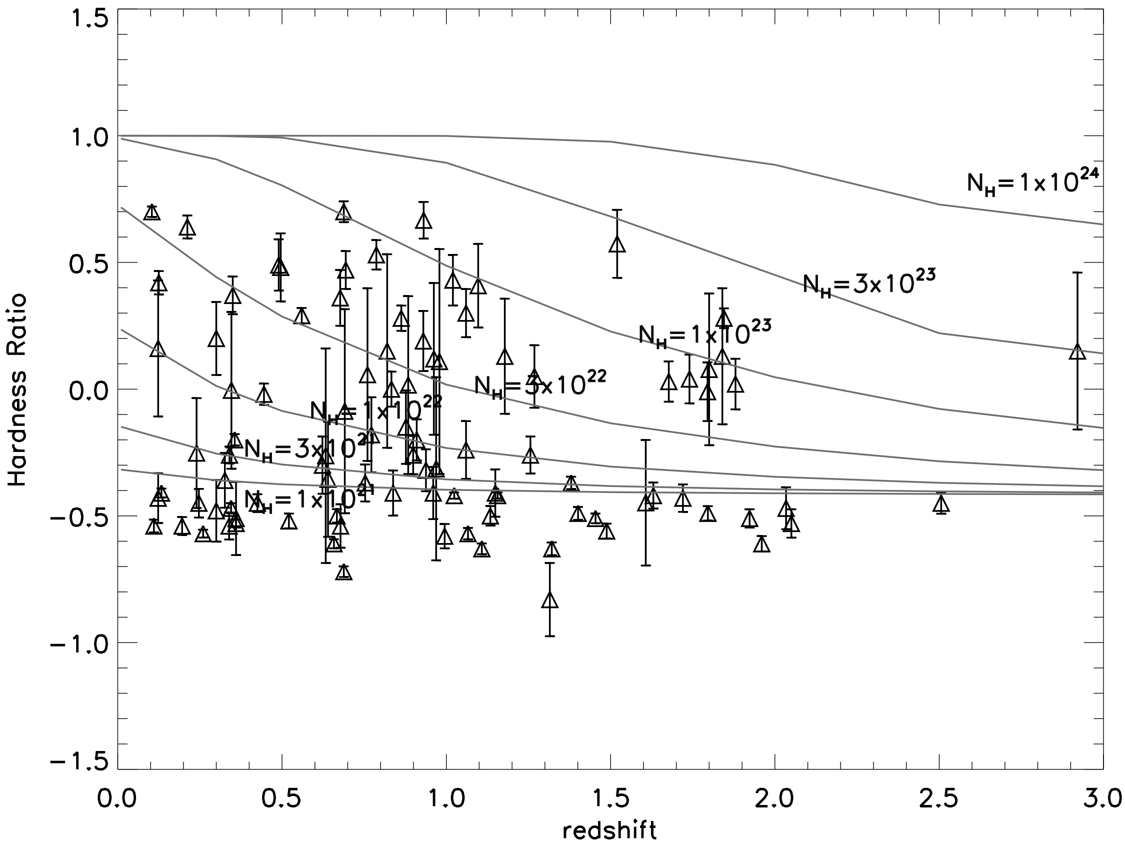

Fig. 4.— The hardness ratio (HR) versus redshift of 70μm/X-ray galaxies. Error bar indicates 1 σ dispersion from either XMM or Chandra catalogs. The solid lines from bottom to top present different amount of N_H = 1 x 10^{21}, 3 x 10^{21}, 1 x 10^{22}, 3 x 10^{22}, 1 x 10^{23}, 3 x 10^{23}, and 1 x 10^{24} cm^{-2}, respectively. Because of negative k-correction effect in X-ray wavelength, higher energy photon can penetrate a large amount of neural hydrogen indicates the HRs decrease with increased redshift. The HR value below the -0.5 indicates there is no obscuration in X-ray emission.

attempted to use HRs as an indicator for column density of N_H along light-of-sight that could provide the clue to derive unabsorbed hard X-ray luminosity. First, in order to prevent degeneracy among photon index and column density, we fixed the intrinsic photon index of power law to 1.7 as general broad-line AGN. To simulate the observed HRs, we used *Portable, Interactive, Multi-Mission Simulator* (PIMMS)[4] from HEASARC and set a fake source with varied amount of N_H, covering a redshift interval 0 < z < 3. Then comparing the expected HRs to those well-defined ones (96/142; ∼ 68%), we could obtain the appropriate quantity of column density. Figure 4 displays the value of HR versus the redshfit, the solid lines from bottom to top present different amount of N_H = 1 x 10^{21}, 3 x 10^{21}, 1 x 10^{22}, 3 x 10^{22}, 1 x 10^{23}, 3 x 10^{23}, and 1 x 10^{24} cm^{-2}, respectively. The mean value of HR for 70μm/X-ray galaxies in COSMOS field is -0.16 with corresponding N_H = 2.7 x 10^{22} cm^{-2}. The histogram of N_H for 70μm/X-ray galaxies is shown in Figure 5.

Second, we inputted the best-fit column density with known redshift and the assumption of photon index $\Gamma \sim 0.7$, we could measure the correction factor between absorbed and unabsorbed hard X-ray luminosity for well-defined HR 70μm/X-ray galaxy. Figure 6 shows the absorption correction factor versus redshift, the mean value of F_{rest}/F_{obs} is about 1.05. In fact, the intrinsic rest frame 2-10keV X-ray luminosity is strongly dependent upon the precise quantity of absorption and initial photon index (Γ) assumption (Comastri 2004).

To ensure the intrinsic 2-10keV luminosity robustness, we only estimated the absorption correction for those samples that have both soft and hard band X-ray detection. Similarly, in the latter statistical analyze, we have excluded any sample with no counts in hard band or soft band (i.e. HR = -1 or 1). However, if we set a flux limit as lower limit, lacking soft band counts samples (i.e. HR = 1) could imply the presence of Compton thick

[4]http://heasarc.gsfc.nasa.gov/Tools/w3pimms.html

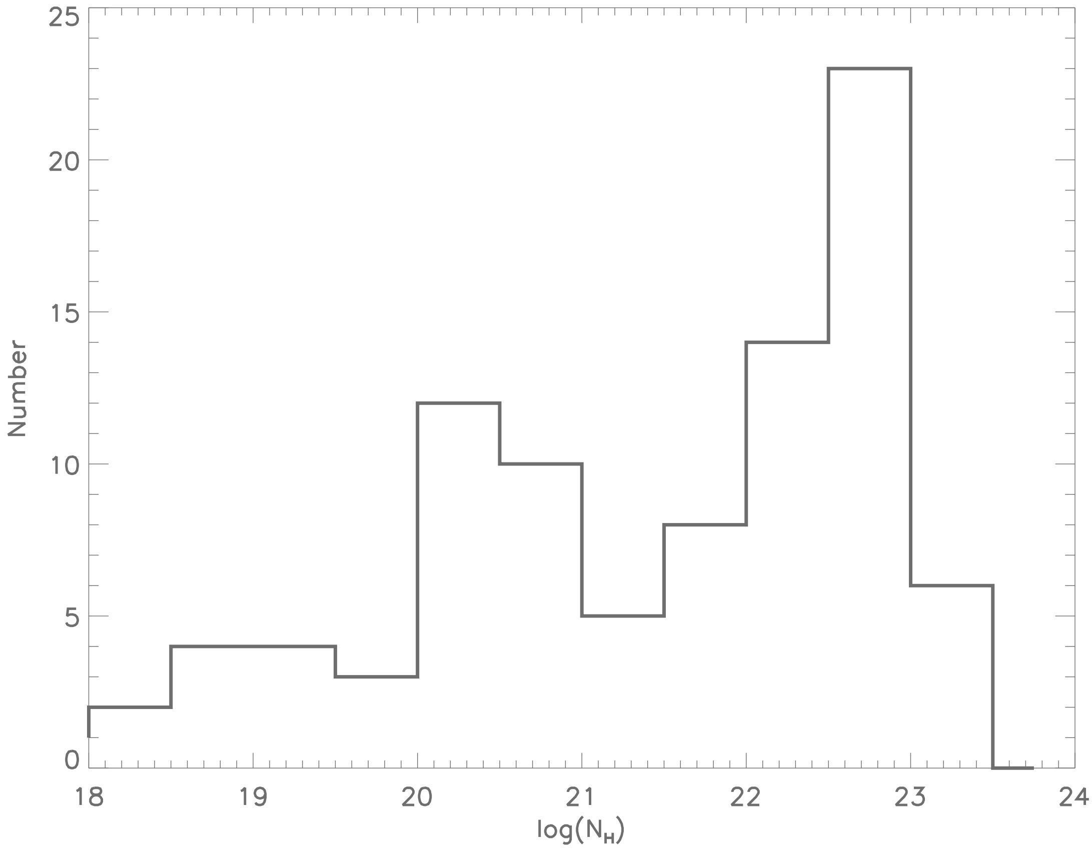

Fig. 5.— The histogram of N_H for 70μm/X-ray galaxies. The column density of neutral hydrogen is derived from well-defined HRs by assuming photon index (Γ) = 1.7. The mean value of HR for 70μm/X-ray galaxies in COSMOS field is 2.7 x 10^{22} cm^{-2}. The samples with $N_H <$ 1.0 x 10^{21} cm^{-2} are not shown in Figure 4 because they are derived from extrapolation.

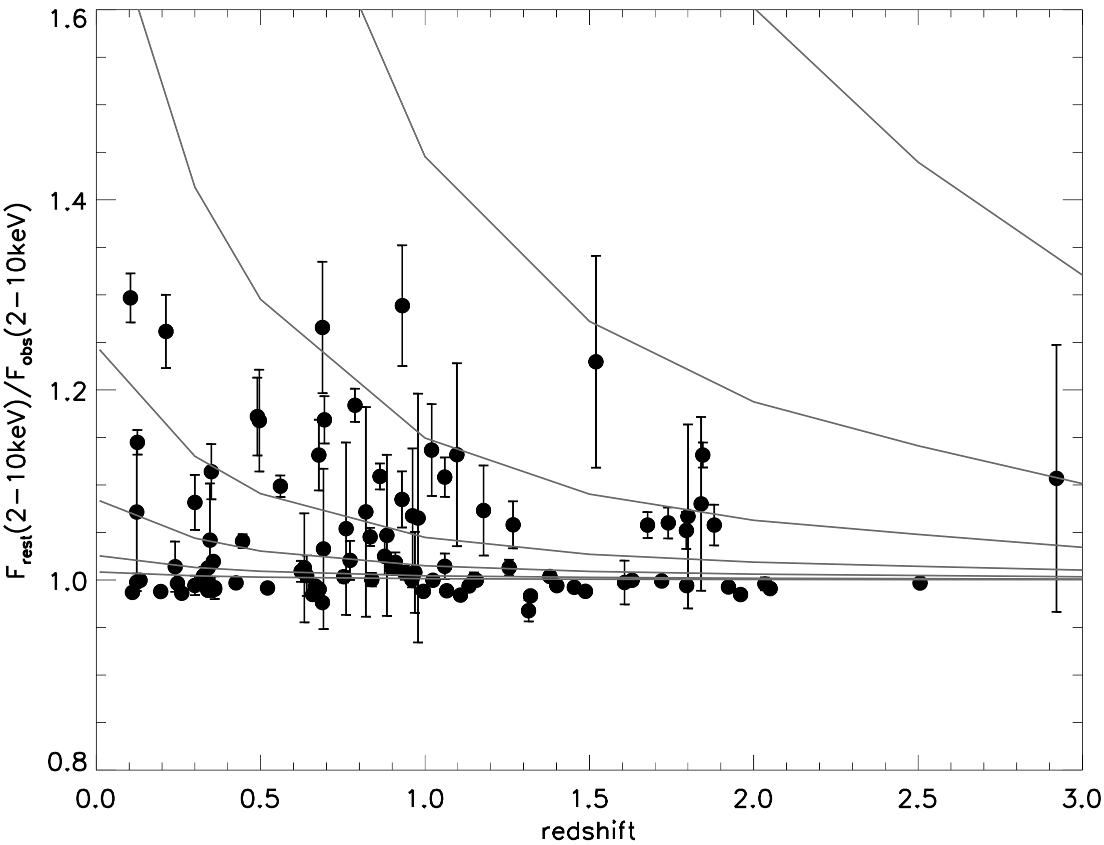

Fig. 6.— The absorption correction factor (F_{rest}(2-10keV)/F_{obs}(2-10keV)) versus redshift. Error bar comes from 1 σ dispersion of HR. The solid lines from bottom to top present different amount of N_H = 1 x 10^{21}, 3 x 10^{21}, 1 x 10^{22}, 3 x 10^{22}, 1 x 10^{23}, 3 x 10^{23}, and 1 x 10^{24} cm^{-2}, respectively. Absorption correction factors with < 1 are set to 1.

AGNs (1 x $10^{24} > N_H$), a notable population in X-ray background synthesis model for the interpretation of intensity peak about 30 keV (Comastri 2004). We will discuss the samples with lacking soft X-ray emission in section 4.3. Previous studies have shown that the star-forming galaxies and infrared excess galaxies are likely to host Compton-thick AGN (Daddi et al. 2007; Fiore et al. 2008). But, in this paper, our aim is to study the mutual influence between AGN and host galaxies with 70μm and X-ray selected technique rather than finding the heavily obscured AGNs.

4. RESULTS

4.1. An AGN or star formation dominated sample?

Our sample is drawn from both 70μm and X-ray catalogs, it is possible that the X-ray luminosity is attributed to a combination of emissions from supernovae remnant, high mass X-ray binaries (HMXBs), and low luminosity AGNs, instead of being generated by a single powerful AGN. For the low X-ray luminosity galaxies, it is difficult to identify the origin of X-ray emission. For instance, Arp220 is considered as the typical ULIRG dominated by star formation. However, the detection of high ionization Fe K lines in its X-ray spectrum prevents us from completely ruling out the possibility of a low luminosity AGN (Iwasawa et al. 2009).

Potentially, Ultraluminous X-ray sources (ULXs, X-ray point source; $L_{\rm X} \geq 10^{39}$ erg s^{-1}) could explain the presence of X-ray emission in a star-forming galaxy. The presence of ULXs are mainly good indicators of recent star formation. However, deeper X-ray observations of Arp220 ruled out any ULX sources detection, in contradiction to the current scenario of recent starburst. A plausible interpretation is that ULXs may be embedded in dust, preventing them from being detected in X-ray survey (Smith et al. 2012).

In this paper, we still define Arp220 as a star-forming ULIRG, as it is commonly done in the literature. Also, we are using Mrk231 as an archetype for AGN ULIRG, as indicated by its strong X-ray emission.

4.1.1. AGN criterion from color-color selection

Mid-infrared IRAC color-color selection described by Stern et al. (2005, hereafter S05) is one of methods to select the AGN candidates. Such color criteria are efficient to separate AGN candidates from star-forming galaxies, due to the red [3.6μm] – [4.5μm] color inferred by the combination of the power law continuum spectrum of the AGN and the relative weakness of the stellar bump feature at 1.6μm usually emitted by the host galaxy. Lacy et al. (2004) proposed another AGN diagnosis using a different IRAC color-color selection from S05. However, Choi et al. (2011) used complete AGN samples, based on the different selections (e.g. BPT diagram, [O III]/Hβ ratio, high excitation line [Ne V], and broad line region feature), to show that the S05 color-color selection is more robust than Lacy et al. (2004).

In Figure 7, we show the IRAC [3.6μm]-[4.5μm] vs. [5.8μm]-[8.0μm] color-color diagram of our 70μm/X-ray galaxies. The deep pink line indicates the AGN dominating region defined by S05. Using these criteria, we separated AGNs from our star-forming galaxies, LIRGs, and ULIRGs. Their estimated AGN fraction is 20% (4 out of 20; blue stars), 48% (29 out of 60; green square), and 92% (57 out of 62; red cross), respectively. There are 63% (90 out of 142) of 70μm/X-ray galaxies classified as AGN from the S05 selection criteria. We remark also that ULIRGs are overlapping more with AGN region in the diagram than the locus of star-forming galaxies; this result is consistent with literature that demonstrates an increasing infrared luminosity as the AGN fraction increases (Lee et al. 2010; Wang et al. 2010).

Our galaxy sample is spanning a wide range of redshifts which may influences the color-color properties due to k-correction effect. To better quantify this redshift effect, we placed the SED of Mrk231 and Arp220 in different redshifts, from z = 0 to z = 3, and monitored the color changes in Figure 7. Templates for Mrk231 and Arp220 are representative of AGN-dominated and star-forming dominated ULIRG, respectively. The Mrk231 colors never leave the S05 AGN region at any redshift because of its featureless power-law SED in mid-IR, while the Arp220 colors do not follow the S05 AGN criteria because the 3.3μm, 6.2μm, and 7.7μmPAH emission lines entering into the IRAC photometry bands.The S05 criteria are therefore not extremely robust against Arp220-like star formation dominating ULIRG.

4.1.2. L_{X} vs. L_{IR} relation

The relation between hard X-ray luminosity and total infrared luminosity provides us with another method to determine whether star formation from host galaxy or AGN predominates the overall SED. While color-color selection can be altered by the presence of specific lines (Donley et al. 2008), total infrared luminosity is more robust because it is derived from 8-1000μm continuum (Smail et al. 2011).

In Figure 8 we display the intrinsic rest frame hard X-ray $(2 - 10\mathrm{keV})$ luminosity against total $(8 - 1000\mu\mathrm{m})$ infrared luminosity for our 70μm/X-ray galaxies, according to their L_{IR} luminosity, subdivided into three sub-samples: star-forming galaxies, LIRGs, and ULIRGs (same symbols as in Figure 7). The hard X-ray luminosity has been rectified N_H absorption according to HRs and k-correction, totally, there are 116 sources have hard X-ray detection, and 96 out of 116 (91%) have well-defined HRs that we could measured intrinsic rest-frame 2-10keV luminosity (absorption correction and k-correction detail, please see Section 3.5). The X-ray luminosity versus Infrared luminosity plot shows a

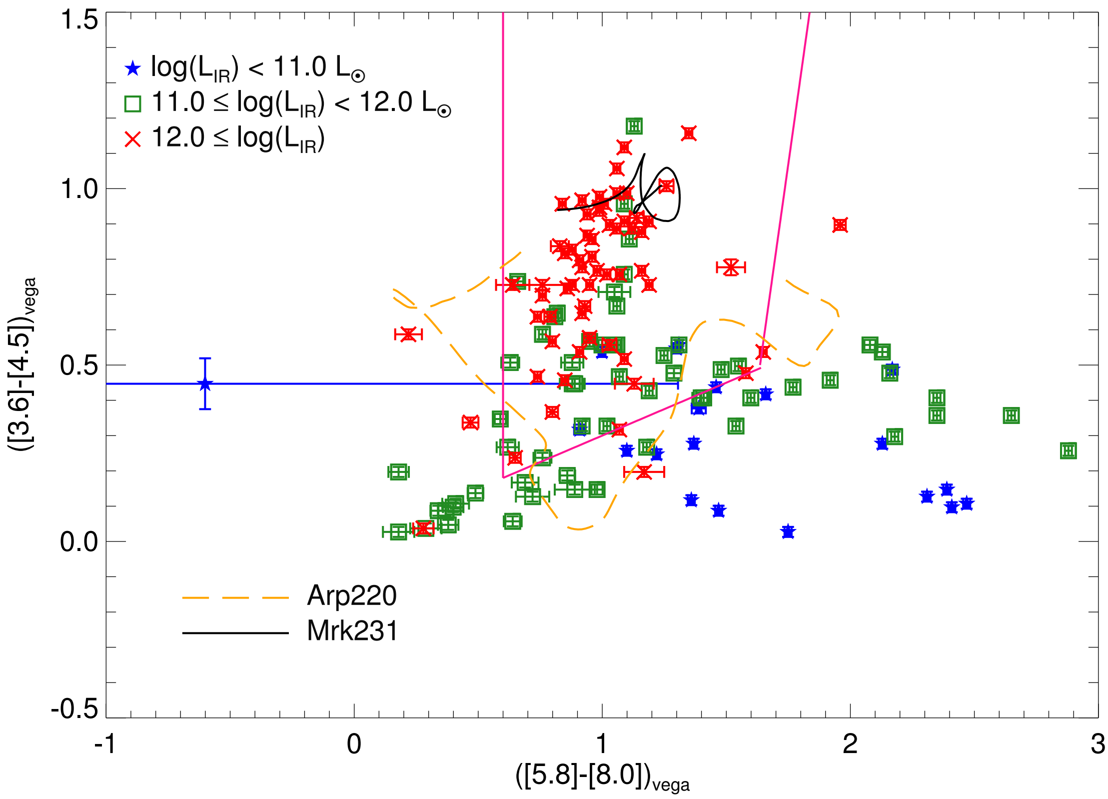

Fig. 7.— [3.6]-[4.5] versus [5.8]-[8.0] color-color diagram of 70μm galaxies with X-ray detection. The different $L_{\rm IR}$-selected galaxy sample follow the description of Figure 1, with blue stars, green squares and red cross indicating star-forming galaxies, LIRGs and ULIRGs respectively. The pink solid continuous line represents the boundaries of the AGN region defined by Stern et al. (2005). Orange dash line and black solid line represent the evolution with redshift from $z = 0$ to $z = 3$ of the colors of Arp220 and Mrk231 templates, respectively. The S05 criterion are not efficient in separating AGNs and Arp220-like star-forming dominated ULIRGs.

tight correlation with Spearman's $\rho \sim 0.88$. However, this strong correlation may be a manifestation of an observational bias. To confirm this, we need to estimate the upper and lower limits in the $L_{\rm X}$ vs. $L_{\rm IR}$ plot. In the case of the total infrared luminosity, we slice the whole 70μm catalog (Kartaltepe et al. 2010) into several redshift bins from z = 0.033 to z = 3, and identify the maximum and minimum total infrared luminosity. For the hard X-ray luminosity, we simulate the lower X-ray luminosity in the same redshift bins using the Chandra flux limits, and measure the upper X-ray luminosity directly from the XMM catalog (Brusa et al. 2010). The results are displayed as gray regions in Figure 8. These observational limits and their evolution with redshift indeed explain the tight correlation between the infrared and X-ray luminosities.

By studying X-ray properties of star-forming galaxies, Ranalli et al. (2003) demonstrated that hard X-ray luminosity is also proportional to star formation rate (SFR). In fact, the most important contributors of X-ray emission in such galaxies are the high mass X-ray binaries (HMXBs). Franceschini et al. (2003) explored the X-ray properties of a sample of ULIRGs; most of them are without AGN signature. The conclusion of their work is that the X-ray luminosity and spectral shape of some ULIRGs are dominated by hot thermal plasma and X-ray binaries, originated in recent starburst region.

On the other hand, because of the presence of the parsec-scale dust "torus" surrounding the accretion disk of the central SMBHs, AGNs emit light in the infrared wavelength (Gandhi et al. 2009). Indeed, the ultraviolet and optical light emit by the central accretion disk is absorbed by the dust and reemit in infrared. Gandhi et al. (2009) observed the core of nearby AGNs with unprecedented high spatial resolutions in both mid-IR and X-ray wavelength, demonstrated a strong correlation between 12.3μm and hard X-ray luminosities without the star formation perturbation from host galaxy. Although observed frame in 12.3μm would influenced by PAH 11.3μm line in Gandhi et al. (2009) samples, the

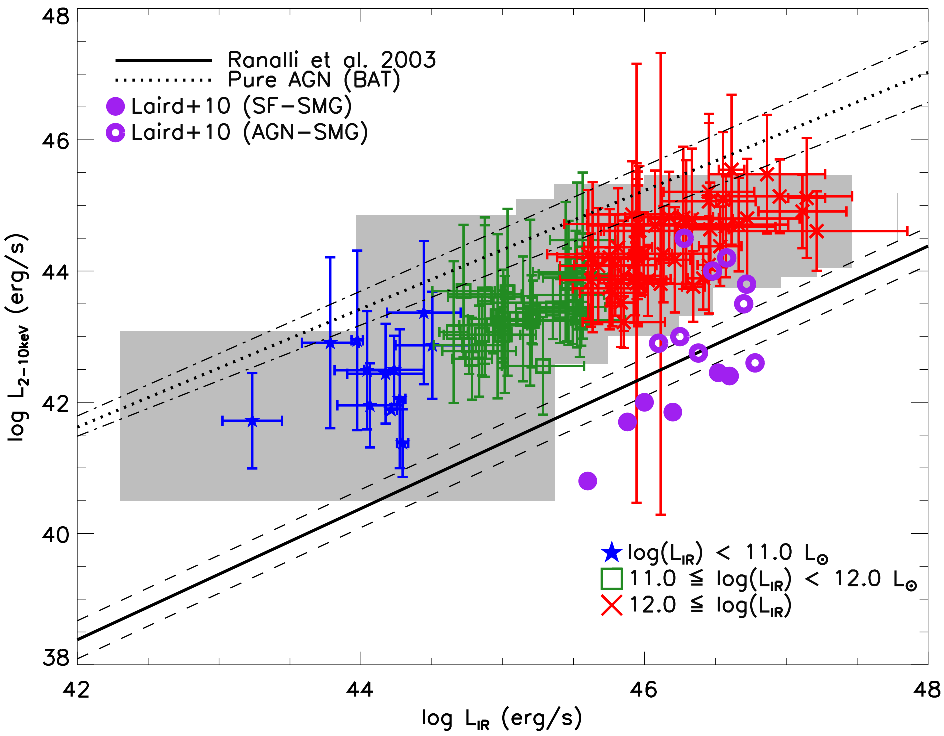

Fig. 8.— Absorption-corrected rest frame 2-10keV luminosity versus total infrared luminosity of 70μm selected galaxies with X-ray detection. Symbols are the same than in Figure 7. The X-ray luminosity error bars are derived from the estimated flux errors and the total infrared luminosity error bars are derived from the 1σ probability distribution of the χ^2 SED fitting. Gray regions represent the areas covered by maximum and minimum luminosities in different redshifts bins drawn from the full X-ray selected and and 70μm selected samples. These observational limitations are inducing the apparent strong correlation between $L_{\rm X}$ and $L_{\rm IR}$ observed in in COSMOS field. Black dot line and black solid line represent the $L_{\rm X}$ vs $L_{\rm IR}$ relations for pure AGN and and star-forming galaxy samples, respectively. Dash-dot line and dash line represents 1 σ dispersion of AGN and star-forming equations (Mullaney et al. 2011; Ranalli et al. 2003). The luminosity of star forming submillimeter galaxies (SMGs) and AGN SMGs, base on their X-ray spectrum fitting, are represented by filled and open purple circles receptively (Laird et al. 2010).

small value of dispersion would may be due to statistical uncertainty rather than physical reasons (Lutz et al. 2004). Based on the intrinsic AGN/quasar IR SED from Netzer et al. (2007), Mullaney et al. (2011) related the 12.3μm luminosity to the total infrared luminosity ($L_{\rm IR}$) (their equation 5). By combining the Gandhi et al. (2009) and Mullaney et al. (2011) relations, we derived the unbiased $L_{\rm X}$ vs. $L_{\rm IR}$ relation for AGNs, free of any contamination from the host galaxy. This "pure" AGN $L_{\rm X}$ vs. $L_{\rm IR}$ relation is represented by the dotted line in Figure 8. Such relation has been confirmed by swift-BAT X-ray selected AGN population (Tueller et al. 2010), together with IRAS infrared measurements (BAT/IRAS AGN). The energy band of 14-195keV in swift-BAT observation could select the galaxies with independent of obscuration. Indeed, their 60μm luminosity is more likely to be powered by the AGN rather than star formation activity from the host galaxy because of linearly increasing correlation between $L_{\rm IR}$ and $L_{\rm X}$ (Mullaney et al. 2012). For our COSMOS sample, the $L_{\rm X}$ vs. $L_{\rm IR}$ distribution of 70μm/X-ray galaxies deviates from AGN relation and star forming relation by $0.5 - 1$ dex and $1 - 2$ dex, respectively. From the infrared and X-ray continuum perspective, AGNs approximately dominate the entire system.

Submillimeter galaxies (SMGs) are a population of objects selected according to their detection in submillimeter wavelengths. This population is dominated by strongly star-forming galaxies at high redshift, with this star formation producing a large amount of cold dust (Chapman et al. 2005). The concomitance in redshifts and infrared luminosities with ULIRGs indicates that SMGs may be an early stage of evolution of the merger scenario (Greve et al. 2005; Biggs & Ivison 2008; Engel et al. 2010). Ultra-deep X-ray observations for those distant star-forming galaxies indicate that 20-30% of SMGs host an AGN (Alexander et al. 2005). Laird et al. (2010) have studied the X-ray spectral properties of SMGs to classify them as AGN or starburst. These objects are represented in Figure 8 with open and closed purple circles, respectively. Our 70μm/X-ray galaxies appear to share the same L_X vs. L_{IR} relation as the AGN-confirmed SMGs.

In summary, all indicators in the L_X vs. L_{IR} distribution of our 70μm/X-ray galaxies cover toward a higher AGN activity relative to star formation.

4.2. Dust temperature of host galaxy

According to the predictions from the merger scenario, galaxy interaction triggers massive star formation, generating large amount of dust, at the same time, it disturbs the gas distribution, funneling it toward the central black hole, feeding the accretion disk, and therefore generating a phase of nuclear activity (Imanishi et al. 2010). If the center of the galaxy harbors an AGN, dust in host galaxy could be influenced by the radiations produced by the nucleus. One way to trace the feedback from AGN, is to observe the galaxy in the far-infrared wavelengths, as they are a good tracer of the dust temperature in the host galaxy (Magdis et al. 2010).

In order to accurately determine the wavelength at the peak of blackbody radiation, and separate several cold dust components with different temperatures, information on the fluxes in the Rayleigh-Jeans tail of the blackbody, hence at longer wavelength, is essential. However, in a simple case, assuming a single blackbody profile with fixed emissivity $\beta = 1.5$ in the Rayleigh-Jeans regime, $F_{70\mu\mathrm{m}}$ and $F_{160\mu\mathrm{m}}$ fluxes are sufficient enough to fit Wien regime of the blackbody. In this simplified case, we could at least derive an upper limit for the cold dust temperature from the limited information (for details of the calculation, see section 3.4).

As shown in Figure 9, the dust temperature of 70μm galaxies correlates strongly with the total infrared luminosity. This is actually an observational bias because of a monochromatic wavelength selection. The far-infrared 70μm selected galaxies with 160μm

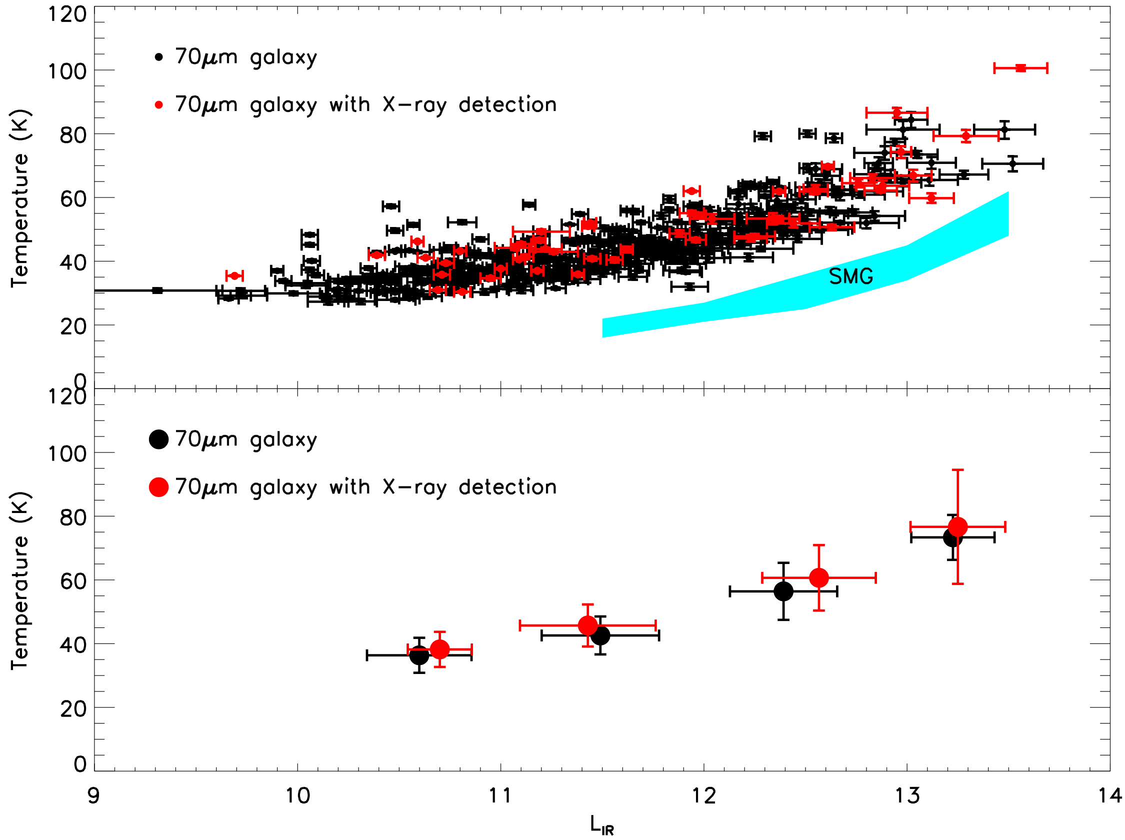

Fig. 9.— *Upper panel* : Luminosity-Temperature diagram; black points and red points refer to all 70μm galaxies and 70μm/X-ray galaxies, with temperatures derived from a single black-body fit with fixed emissivity. Both total infrared luminosity and temperature error bars are estimated from the 1σ probability distribution of the χ^2 SED fitting. Temperatures depend strongly of redshift, given it was estimated from one photometric band only, which result in warmer temperatures at higher redshifts. Similar effects are observed with the SMG population, whose luminosity-temperature relation is shown as the cyan area, although they have typically lower dust temperature for similar infrared luminosity (Chapman et al. 2005). *Lower panel* : Average temperature for different bins of total infrared luminosity (average from the values of upper panel) in different total infrared luminosity interval; black points and red points refer to all 70μm galaxies and 70μm/X-ray galaxies. The presence of AGN does not enhance the dust temperature of 70μm-selected galaxies.

detection could express the SED of cold dust temperature from host galaxy accurately. Indeed, at higher redshifts, the rest-frame flux corresponds to shorter wavelengths, and therefore probes warmer temperature. A similar incompleteness bias is acting on the estimation of dust temperature for SMGs, the selection at longer wavelengths (observed frame 850μm, i.e. $\sim$ 300μm at $z \sim 2$) probed a lower dust temperature regime (Chapman et al. 2005).

However, incomplete bias have little influence in our comparative study between 70μm-selected with and without X-ray detection. In total, we have estimated the temperature for 463/1503 (31%) of the 70μm-selected galaxies, of which 52/142 (37%) with X-ray detection. Such a large sample of 70μm galaxies with/without X-ray provides a good statistical ground to investigate any difference in dust temperature between AGN and non-AGN galaxies.

In Figure 9, 70μm galaxies with/without X-ray detection are labeled as red/black filled circles, respectively, with the error bars estimated from the 1σ probability distribution of χ^2 fit. Although 70μm/X-ray galaxies display systematically slightly higher dust temperature compare to non-X-ray detected 70μm galaxies (a shift of 2-4K for a temperature of 36-73K), the difference is not significant given the large uncertainties in the measurements (between 6K and 18K). Therefore, we do not observe any noticeable discrepancy of the presence of AGN on the dust temperature of the host galaxy, suggesting the far-infrared emission from AGN-hosted galaxies similar to star formation, in agreement with the recent observations based on Herschel far-infrared result from Elbaz et al. (2010).

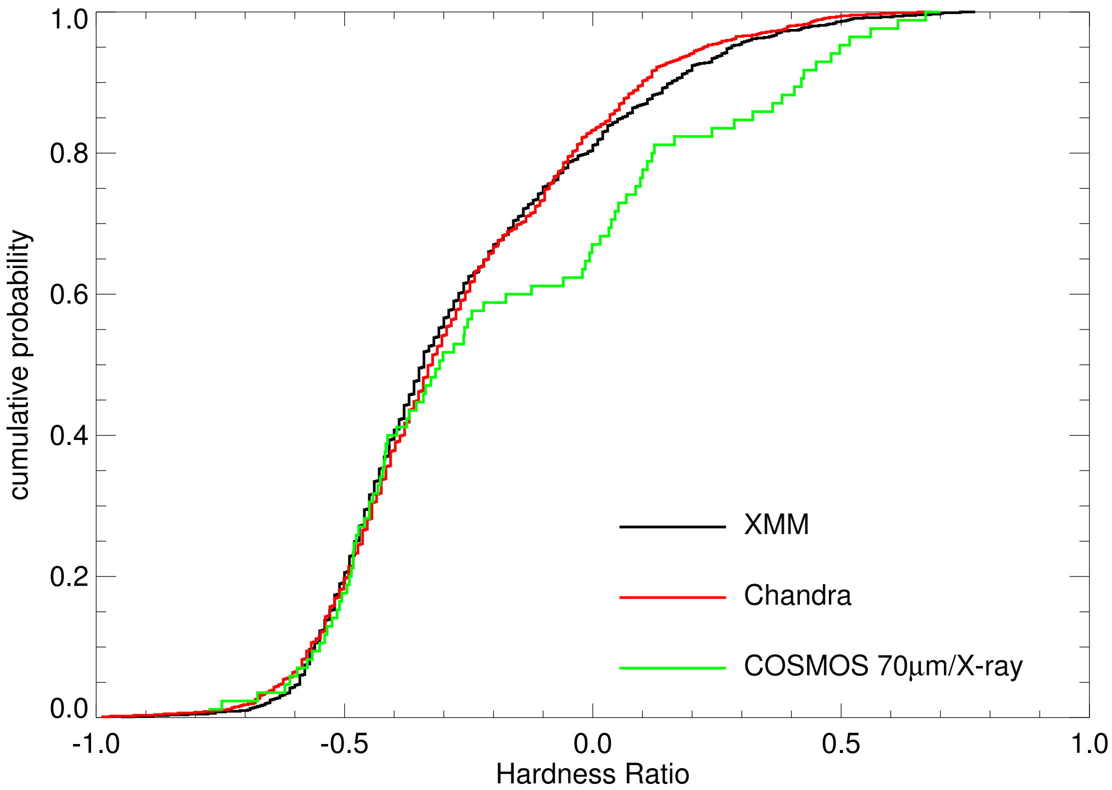

Fig. 10.— Kolmogorov-Smirnov test: the hardness ratio cumulative probability distribution of XMM, Chandra, and 70μm/X-ray selected galaxy samples represented in black, red, and green color lines respectively. Distribution of XMM and Chandra indicates these samples are drawn from the same population. However 70μm/X-ray galaxies seems not drawn from the same population than purely X-ray selected samples. The distribution indicates an excess of HR at $\geq$ -0.3, revealing that the cold dust from the host starburst galaxy me be responsible of additional obscuration.

4.3. Hardness ratio of 70μm/X-ray galaxies

To explain the diversity of AGNs (e.g., narrow-lines vs. broad-lines), a unified model, based on the variation of obscuration due to the orientation of the dust torus surrounding the SMBH accretion disk, has been proposed. In such model, the presence of an edge-on dust torus not only blocks the broad-line emissions, but also increases the absorption in soft X-ray because of the higher hydrogen column density (Antonucci 1993).

In addition, for on-going galaxy mergers, the star formation trigger the additional amount of neutral hydrogen formation, absorbing soft X-ray (e.g., Esquej et al. 2012). Indeed, using the Extended Chandra Deep Field-South (ECDF-S) dataset, Treister et al. (2009) observed large obscuration of the soft X-ray emission in star-forming galaxies hosting an AGN at high redshifts, revealing a large amount of neutral hydrogen on the line-of-sight.

Our aim is investigating if there is a direct connection between the obscuration properties of the AGN and those of the host galaxy. As absorption affects the soft X-ray emissions more than the hard X-ray emissions, the HR is a good tracer of obscuration, with higher value of HR corresponding to larger absorption. To test whether our two samples, X-ray selected galaxies and 70μm/X-ray galaxies, are consistent with being drawn from the same sample (i.e. our null hypothesis), we apply Kolmogorov-Smirnov (K-S) test (*Numerical Recipes*, Press et al. 1992).

As an initial test, we examined the HR of XMM and Chandra X-ray selected sources, to test the robustness of our conversion between XMM HR and Chandra HR (conversion factor for Chandra HRs, see section 3.4). The results of our K-S test for these populations are shown in Figure 10, with the HR cumulative probability distribution of XMM selected sample in black solid line and Chandra selected sample in red dotted line, and the K-S parameters are summarized in Table 3. The probability is only 3% that XMM sample and Chandra sample are drawn from same parent samples, which is not significant enough to reject the null hypothesis (our threshold to reject the null hypothesis is 99%). Although two X-ray facilities have different sky coverage and depth, XMM HR distribution is roughly identical to the Chandra HR distribution.

Then, we apply the K-S test between the 70μm/X-ray and XMM samples. This time, the null hypothesis is rejected at a significance of 99% confidence level, implying that 70μm/X-ray galaxies and XMM galaxies are drawn from different populations. The K-S test between 70μm/X-ray and Chandra selected samples also rejects the hypothesis. The probability of drawing from same population for XMM & 70μm/X-ray is $\sim$ 0.3%, for Chandra & 70μm/X-ray is 0.2%. Figure 10 displays the cumulative probability distribution of HR from XMM (black solid line), Chandra (red solid line), and 70μm/X-ray (green solid line) selected samples. The K-S parameters resulting from the three tests are summarized in Table 3.

In fact, the probability distribution fraction below HR $\leq$ 0.3 of XMM, Chandra, and 70μm/X-ray galaxies is similar, indicates the unobscured AGN fraction is uniform. The obvious diversity appears above the HR > -0.3, in terms of the probability distribution of XMM and Chandra, there is 80% AGNs with HR $\leq$ 0, however, there is only 60% AGNs with HR $\leq$ 0 from 70micron/X-ray selection. According to column density derived from HR, the mean value of N_H for overall 70μm/X-ray galaxies corresponds to 10^{22} cm^{-2} which is consistent with mildly absorbed AGN population definition. But there are 21 70μm/X-ray galaxies lacking in soft X-ray among our sample, which could be candidates of Compton thick AGN we did not count in K-S tests. In order to derive the column density for lacking soft X-ray detection 70μm/X-ray galaxies, we assumed their soft X-ray count rate from flux limit, and then calculated the hardness ratio as a lower limit. Applying the same method (section x.x), we obtain the mean value of column density is at least $\sim 10^{23}$ cm^{-2} for 21 out of 70μm/X-ray galaxies. From lacking soft X-ray detection sample, there is one object

(X-ray ID = 5042, 70μm ID = 1539) could be a Compton thick AGN ($N_H \sim 1.45$ x 10^{24} cm^{-2}), its photometric redshift corresponds to 2.36 with total infrared luminosity exceed 10^{13} L$\odot$, belonging to hyper ULIRG. Even we neglected the lacking soft X-ray detection 70μm/X-ray galaxies, the K-S tests for well-defined HR 70μm/X-ray galaxies is significant enough to show there is additional neutral hydrogen exists with 70μm/X-ray selection.

The tests indicate that 70μm/X-ray galaxies include more obscured AGNs than purely X-ray selected samples. This implies that, in the case of AGNs hosted by dust-enshrouded galaxies, the presence of dust would not only associated to AGN unified model scheme but also additionally physical process. Furthermore, the N_H of dust-enshrouded galaxies from 70μm/X-ray selection is not heavily obscured like Compton thick AGNs, predicted from X-ray background synthesis. We speculate that the excess of obscuration is not only attributed to absorption on the line-of-sight by continuum or clumpy dust torus around the SMBH, but also is associated with an additional more diffuse dust component generated by strong star formation in the host galaxy. The starburst can be subsequence of an event involving the whole system (e.g. merger) or generated by the circumnuclear region (e.g. bar). Because of tight symbiosis between AGN and host galaxy, hence we can not neglect the influence of the host galaxy on AGN properties. Only X-ray observations with very high spatial resolution will enable us to identify the origin of the extra amount of neutral hydrogen.

5. DISSUSSION

5.1. AGN influence on the host galaxy dust temperature?

Our analysis in section 4.2 demonstrates there are no connection between cold dust temperature and the presence of AGN, in agreement with recent result (e.g. Elbaz et al.

Table 2: Confirmed spectroscopic redshift sample

Telescope	Instrument	$N^{(a)}$	Reference
ESO-VLT	VIMOS	49	zCOSMOS
			Lilly et al. (2007)
Magellan	IMACS	26	Trump et al. (2007)
Sloan	SDSS	15	Abazajian et al. (2009)
Keck II	DEIMOS	11	Kartaltepe et al. (2010)
MMT	Hectospec	1	Prescott et al. (2006)

$^{(a)}$Number of 70μm/X-ray sources with spectroscpic redshift.

Table 3: Results of the K-S test on the hardness ratio between different catalogs

Catalogs	$D_{\rm max}$	Significant level	Hypothesis
XMM & Chandra	0.06637	0.0279	Not Reject
XMM & 70μm/X-ray	0.1920	0.0026	Reject
Chandra & 70μm/X-ray	0.1981	0.0018	Reject

2010). This result could attribute to the spatial scale problem, the cold dust component is so far away from the central energetic source that is insufficient for heating the cold dust component.

Rafferty et al. (2011) used infrared color $\log(F_{24\mu}\mathrm{m}/F_{70\mu}\mathrm{m})$, to sample the blackbody temperature profile and concluded that galaxies hosting an AGN present a high dust temperature, which is inconsistent with our temperature fitting result. We reproduced their analysis for our sample, as shown in Figure 11. The 70μm/X-ray galaxies present a higher color index in average than overall 70μm galaxies at all redshifts, a same conclusion to Rafferty et al. (2011). Though the 70μm/X-ray galaxies show higher $\log(F_{24\mu}\mathrm{m}/F_{70\mu}\mathrm{m})$, they still agree with the local definition of cold dust (e.g. $\log(25/60) < 0.2$ de Grijp et al. 1985; Sanders et al. 1988b).

To explain the difference in color index, we looked at the evolution of the $F_{24\mu}\mathrm{m}/F_{70\mu}\mathrm{m}$ color as a function of the redshift for two typical objects, the star-forming ULIRG Arp220 and the AGN ULIRG Mrk231. We used the galaxy templates provided by Polletta et al. (2007), as shown in Figure 11. In the case of Arp220, the rest frame 9.7μm absorption line is shifted into the 24μm band at redshift $z \sim 1.5$, causing an apparent lower value of the color index. Similarly, at $z > 2$, the 7.7 and 8.2 μm PAH emission lines are entering the 24μm band, inducing a higher $F_{24\mu}\mathrm{m}/F_{70\mu}\mathrm{m}$ color ratio. In the case of Mrk231, the AGN driven power-law continuum produces a more stable color index. Our 70μm/X-ray samples follow the same color index of Mrk231-like galaxies across the redshift range $0 < z < 3$, and the remaining parts of our samples follow more a Arp220-like profile. We supported the idea that the $F_{24\mu}\mathrm{m}/F_{70\mu}\mathrm{m}$ color is sensitive to hot dust component from nearby region of AGN, on the other hand, for the longer wavelength (e.g. Elbaz et al. (2010) and our temperature fitting work), it would respond to the cold dust temperature from star formation in host galaxy. We summarized that the color of $F_{24\mu}\mathrm{m}/F_{70\mu}\mathrm{m}$ and temperature fitting trace different temperature components of dust, the 24μm is sensitive to warm dust around AGN, therefore we can see the discrepancy of color in X-ray detected 70μm galaxies. On the other hand, the temperature fitting method and Elbaz et al. (2010) work included the longer wavelength of SED, star formation dominated the cold dust whether the AGN presence or not.

To have a robust measurement of the variation of dust temperature in the host galaxy, we need to explore the longer wavelengths that have less perturbation from emission (e.g. 8.6 μm and 11.2 μm PAH lines) and absorption (e.g. 9.7 μmsilicate line) line features. For instance, measuring the longer wavelength color (e.g. $F_{70}\mu\mathrm{m}/F_{160}\mu\mathrm{m}$) is a more accurate method to estimate the dust temperature (Casey 2012). We compared the value of $F_{70}\mu\mathrm{m}/F_{160}\mu\mathrm{m}$ between X-ray detected and X-ray undetected 70μm galaxies, for those lacking 160μm measurement 70μm galaxies, we applied upper limit from flux limit as their $F_{160}\mu\mathrm{m}$ monochromatic photometry . The K-S test shows that is 9% draw out of the same population, we cannot rule out they originate from the identically parental sample, this conclusion is consistent with temperature fitting result.

In order to simplify the temperature fitting, the models of temperature usually assume that β is a constant value. However, it depends on which photometric bands are included; shorter wavelength photometry will induce the lower β value, and probe a systematically higher temperature (Magnelli et al. 2012). Our fitting procedure provides no strong evidence that the cold dust of host galaxy is related to AGN (see section 4.2). Such result is consistent with the latest work from the Herschel observations (Elbaz et al. 2010). Actually, the photometry in the 250μm, 350μm, and 500μm bands provides information on the Rayleigh-Jeans portion of the spectra, and therefore enables a more accurate estimation of the dust temperature of the host galaxy. Such precise measurements show a $2-3$K differences between the dust temperature of a galaxy with AGN and without AGN (Elbaz

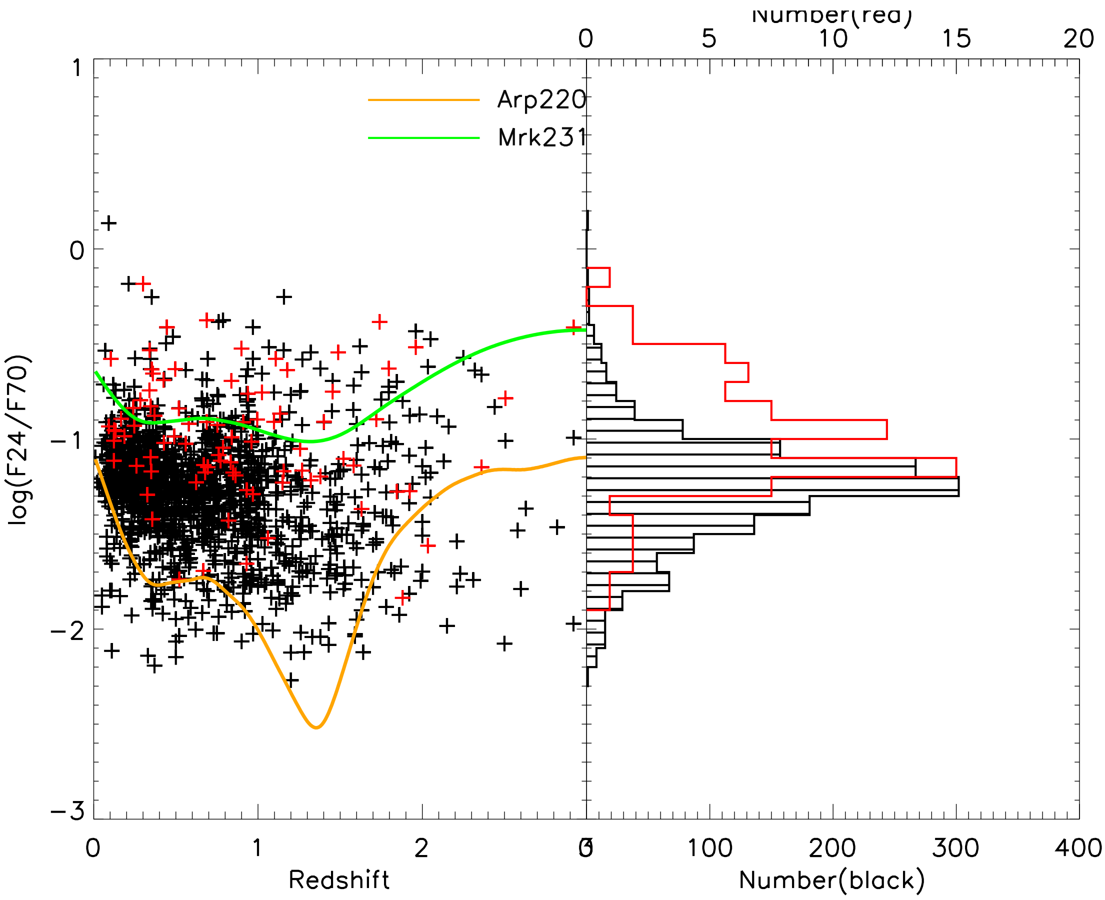

Fig. 11.— Distribution of $\log(F_{24\mu m}/F_{70\mu m})$ color index for 70μm selected sample and 70μm/X-ray sample. *Left panel* : Distribution of the color against redshift for the 70μm galaxies (black crosses) and the 70μm/X-ray sample (red crosses). The green and orange lines indicate the evolution of Mrk231 and Arp220 flux ratio as a function of redshift, computed using the templates from Polletta et al. (2007). *Right panel* : Histogram of the color index for 70μm-selected galaxies in black and 70μm/X-ray in red, with the red histogram normalized to the peak of black sample for better display (bottom and top axis represent the number of 70μm-selected galaxies and 70μm/X-ray respectively). The 70μm galaxies have a median color index of $\log(F_{24\mu m}/F_{70\mu m}) \sim -1.25$, while for 70$\mu$m/X-ray galaxies it is of ~ -0.99. Both satisfy the local cold dust definition of $\log(F_{24\mu m}/F_{70\mu m}) \leq -0.7$ (de Grijp et al. 1985; Sanders et al. 1988b).

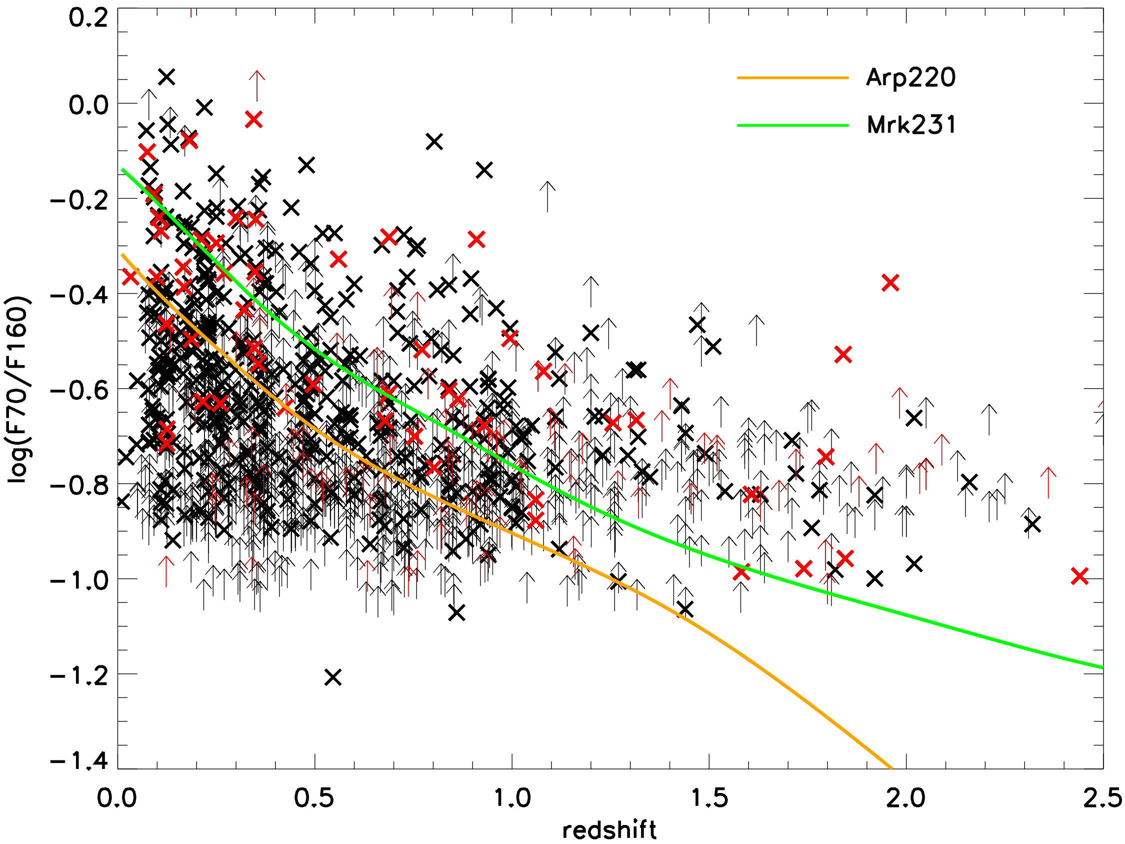

Fig. 12.— The color index of $\log(F_{70\mu\mathrm{m}}/F_{160\mu\mathrm{m}})$ against redshift for 70μm galaxies. The red color and black color is 70μm/X-ray galaxies and 70μm galaxies without X-ray detection, respectively. The cross symbol indicates the 70μm galaxies have 160μm detection, otherwise, the upper arrow symbol indicates the 160μm photometry of those 70μm galaxies is derived from observation limit. The green and orange lines indicate the evolution of Mrk231 and Arp220 flux ratio as a function of redshift, computed using the templates from Polletta et al. (2007).

et al. 2010). The nondistinctive far-infrared colors imply the physical mechanism drives the AGN hosted galaxies is similar to those star forming galaxies.

5.2. AGN obscuration from starburst?

According to the major merger scenario of galaxy evolution, developed to interpret a potential ULIRG-QSO connection, galaxies undergo an obscuration phase after the merger occurred due to an enhancement of star formation and dust production. This obscured phase is thought to be ended by a consecutive AGN phase, during which feedback from the central SMBH repels the dust (Hopkins et al. 2008). Giving an illustration, the NGC 6240, low-ionization nuclear emission-line regions (LINER), is a well-studied ULIRG, with high infrared luminosity indicating a starburst activity that generates a large amount of dust and molecular gas (Iono et al. 2007). A detailed X-ray spectrum from BeppoSAX of NGC 6240 revealed a very strong absorption from the neutral gas column density $N_H \sim 2$ x 10^{24} cm^{-2} (Vignati et al. 1999). Thanks to the higher spatial resolution, Chandra observations of NGC 6240 identified the presence of a double AGNs system, hidden in the core of the galaxy (Komossa et al. 2003). These observations are consistent with the idea that galaxy was formed consequentially of a merger .

To efficiently investigate the evolutionary stages of the AGN concomitance with star formation, our approach is to study the properties galaxies detected in both infrared and X-ray. Rafferty et al. (2011) had a similar approach to ours, looking for the X-ray counterpart of 70μm-selected galaxies in the ECDF-S, CDF-S, and EGS fields. Performing both a X-ray spectrum and a X-ray band ratio analysis, assuming a power-low spectrum derives different column densities, they found the column density derived from X-ray band ratio that are systematically low. From the X-ray spectrum confirmed sample (Tozzi et al. 2006), they did not identify any excess of neutral hydrogen in 70μm-selected X-ray sources compared to other X-ray selected AGNs (Figure 4 in Rafferty et al. (2011) paper). They concluded that the absence of obscured AGN among the star-forming galaxies contradicts to the current AGN and galaxy co-evolution model (Hopkins et al. 2008). Actually, the main reason why Rafferty et al. (2011) did not detect any additional obscured AGN from star-forming galaxies is probably the statistical insufficiency of their sample. Although they have 158 70μm/X-ray galaxies with 108 were identified as AGN, for the purpose of accuracy, they only had accessed to 17 of 70μm/X-ray galaxies, with hydrogen column density NH derived by X-ray spectral analysis, comparing with whole AGN population (Tozzi et al. 2006).

In addition, Rafferty et al. (2011) have used HRs to measure the column density for correcting absorbed X-ray luminosity, most of 70μm/X-ray galaxies with $N_H \sim 10^{20}$ - 10^{23} that is consistent with our mean value of $N_H \sim 10^{22}$. Both Rafferty et al. (2011) and our works have identified one possible Compton-thick AGN comparable to the X-ray properties of ULIRGs in local universe (e.g. Mrk231, NGC6240). We speculated it is due to the selection effect, Compton-thick AGN with large amount of neutral hydrogen that even the hard X-ray photon cannot penetrate. Either checking the Fe Kα line or observing higher energy band in X-ray could seek out more Compton-thick AGNs, however, this issue is beyond our scope of this paper.

Our large sample (142 70μm/X-ray galaxies) enables us a proper statistical study. We therefore took a different approach by applying a K-S test on the distribution of hardness ratio to investigate if 70μm/X-ray galaxies and X-ray selected AGNs are drawn from the same sample (see section 4.3). Trichas et al. (2009) attempted to use the X-ray sources with 70μm counterparts counterparts in the redshift range 0.5 < z < 1.3 from the Spitzer Wide Area Infrared Extragalactic (SWIRE) survey, but they have 3% sufficient probability to conclude that X-ray sources with 70μm detection were drawn from the global X-ray population. In contrast, we used the opposite selection method - 70μm sources with X-ray counterparts since the redshift to 3 in the COSMOS field. Owing to a factor of 2 deeper 70μm observations in the COSMOS field, we could extract a larger sample includes more star forming galaxies with $10^{10}L_{\odot} \leq L_{\rm IR} < 10^{11}L_{\odot}$. Our K-S test shows in less than 0.2% of probability for 70μm galaxies with X-ray detection to be drawn from the global X-ray population. The mean value (1-sigma) of hardness ratio for XMM selected sample, Chandra selected sample, and 70μm/X-ray sample is -0.26 ($\mp$ 0.28), -0.28($\mp$0.29), and -0.16($\mp$0.39), respectively. Such result is in agreement with the merger galaxy formation scenario: the neutral hydrogen obscuration in infrared-luminous AGN not only comes from the dust torus component around the AGN, but also from additionally physical process such as extreme star formation region in the host galaxy.

6. CONCLUSION

We have investigated the properties of 142 galaxies both detected in X-ray and 70μm in the COSMOS field. X-ray data are obtained from both XMM and Chandra point source catalogs, and 70μm photometry is drawn from Spitzer-MIPS 70μm point source catalog. We classified our sample into three distinct subsamples according to their respective total infrared luminosity ($L_{\rm IR}$): star-forming galaxies ($L_{\rm IR} < 10^{11}L_{\odot}$), luminous infrared galaxies (LIRGs, $10^{11}L_{\odot} \leq L_{\rm IR} < 10^{12}L_{\odot}$), and ultra-luminous infrared galaxies (ULIRGs, $L_{\rm IR} \geq 10^{12}L_{\odot}$), with median redshifts of z$\sim$ 0.168, 0.518 and 1.268, respectively. The major conclusions for this study are as follows:

1. We applied two methods to determine which mechanism dominates the SED, star formation or AGN:

   i) Using Spitzer-IRAC colors, we have shown that the majority of our sample is dominated by AGN. Although the higher AGN fraction accompanies with higher total infrared luminosity ($L_{\rm IR}$), the presence of PAH emission lines (e.g. 3.3μm, 6.2μm, 7.7μm, 8.6μm, and 11.2μm) related to star formation could disturb AGN identification.

ii) Using the relation between intrinsic rest-frame hard X-ray (2-10keV) and total infrared luminosity $L_{\rm IR}$ (8-1000μm), we found that our samples are dominated by AGN, with property comparable to AGN detected SMGs.

2. We provided evidences for additional X-ray obscuration in X-ray detected 70μm galaxies, in agreement with current AGN/starburst co-evolution model (Hopkins et al. 2008). A K-S test on the modified HR between 70μm/X-ray galaxies and whole X-ray samples rejected the assumption of them to be originated from the same population within 99% confidence level, supporting the idea that the excess of X-ray absorption does not come from the AGN dusty torus obscuration, but probably from additional diffuse obscuration generated by the star formation in the galaxy.

3. We estimated the dust temperature of our 70μm galaxy samples by fitting their far-infrared photometries with fixed emissivity models. Despite the presence of a warm dust component, the cold dust shows a similar temperature in host galaxy with and without AGN, indicating that the longer wavelengths are still dominated by star formation. This evidence conflicts with a scenario where radiative feedback from the AGN truncates the star formation in the host galaxy.

Acknowledgements

I would like to express my deepest appreciation to all people who help me the possibility to finish this master thesis. I would like to dedicate this thesis to my parents, Grace Chang and Ching-Yuan Lin, for their unconditional supports and allowing me to be as ambitious as I wanted. Thanks to my dog - Pocky, he brings a lot of fun for me through my research process. A great gratitude I give to my supervisors, Yasuhiro Hashimoto and Sébastien Foucaud, who provide plentiful advices and help me to coordinate my project especially in writing this report. A special thanks to Lin-Wen Chen, with his solid training for astronomical courses that inspired me to put more efforts on my master project.

We would like to acknowledge the wonderful work made by Jeyhan S. Kartaltepe on the Spitzer-COSMOS 70μm point source catalog on which our analyses are based. We would like to thank the following people for very useful discussions, suggestions, and comments: Jeyhan S. Kartaltepe, Wei-Hao Wang, Albert Kong, Matthew A. Malkan, Nick Scoville, and David B. Sanders.

The work presented here is supported by the National Science Council of Taiwan under the grants NSC99-2112-M-003-002-MY2, NSC99-2119-M-003-005, and NSC 99-2112-M-003-001-MY2. This research used extensively the COSMOS survey archive data of the NASA/IPAC Infrared Science Archive, which is operated by the Jet Propulsion Laboratory, California Institute of Technology, under contract with the National Aeronautics and Space Administration.

REFERENCES

Abazajian, K. N., Adelman-McCarthy, J. K., Agüeros, M. A., et al., 2009, ApJS, 182, 543

Akylas, A., Georgantopoulos, I., Georgakakis, A., Kitsionas, S., & Hatziminaoglou, E., 2006, A&A, 459, 693

Alexander, D. M., Smail, I., Bauer, F. E., et al., 2005, Nature, 434, 738

Alonso-Herrero, A., Pérez-González, P. G., Alexander, D. M., et al., 2006, ApJ, 640, 167

Antonucci, R., 1993, ARA&A, 31, 473

Armus, L. 2006, Astronomical Society of the Pacific Conference Series, 357, 218

Arnouts, S., Cristiani, S., Moscardini, L., Matarrese, S., Lucchin, F. , et al., 1999, MNRAS, 310, 540

Baan, W. A., Salzer, J. J., & Lewinter, R. D., 1998, ApJ, 509, 633

Baldwin, J. A., Phillips, M. M., & Terlevich, R., 1981, PASP, 93, 5

Balestra, I., Boller, T., Gallo, L., Lutz, D., & Hess, S. 2005, A&A, 442, 469

Barnes, J. E., & Hernquist, L. E. 1991, ApJ, 370, L65

Bauer, F. E., Yan, L., Sajina, A., & Alexander, D. M. 2010, ApJ, 710, 212

Bennert, N., Canalizo, G., Jungwiert, B., et al., 2008, ApJ, 677, 846

Biggs, A. D., & Ivison, R. J., 2008, MNRAS, 385, 893

Boquien, M., Bendo, G., Calzetti, D., et al., 2010, ApJ, 713, 626

Borne, K. D., Bushouse, H., Lucas, R. A., & Colina, L., 2000, ApJ, 529, L77

Braito, V., Della Ceca, R., Piconcelli, E., et al., 2004, A&A, 420, 79

Brand, K., Dey, A., Weedman, D., et al., 2006, ApJ, 644, 143

Brightman, M., & Ueda, Y. 2012, MNRAS, 423, 702

Brusa, M., Civano, F., Comastri, A., et al., 2010, ApJ, 716, 348

Canalizo, G., & Stockton, A., 2001, ApJ, 555, 719

Capak, P., Aussel, H., Ajiki, M., et al., 2007, ApJS, 172, 99

Cappelluti, N., Brusa, M., Hasinger, G., et al., 2009, A&A, 497, 635

Casey, C. M., Chapman, S. C., Beswick, R. J., et al., 2009, MNRAS, 399, 121

Casey, C. M., 2012, MNRAS, 425, 3094

Chapman, S. C., Blain, A. W., Smail, I., & Ivison, R. J., 2005, ApJ, 622, 772

Choi, P. I., Yan, L., Helou, G., et al., 2011, ApJ, 732, 21

Chung, A., Yun, M. S., Naraynan, G., Heyer, M., & Erickson, N. R. 2011, ApJ, 732, L15

Clements, D. L., Dunne, L., & Eales, S., 2010, MNRAS, 403, 274

Comastri, A. 2004, Supermassive Black Holes in the Distant Universe, 308, 245

Cui, J., Xia, X.-Y., Deng, Z.-G., Mao, S., & Zou, Z.-L., 2001, AJ, 122, 63

Daddi, E., Dickinson, M., Morrison, G., et al. 2007, ApJ, 670, 156

de Grijp, M. H. K., Miley, G. K., Lub, J., & de Jong, T., 1985, Nature, 314, 240

Donley, J. L., Rieke, G. H., Pérez-González, P. G., Rigby, J. R., & Alonso-Herrero, A., 2007, ApJ, 660, 167

Donley, J. L., Rieke, G. H., Pérez-González, P. G., & Barro, G., 2008, ApJ, 687, 111

Elbaz, D., Hwang, H. S., Magnelli, B., et al., 2010, A&A, 518, L29

Elvis, M., Civano, F., Vignali, C., et al., 2009, ApJS, 184, 158

Engel, H., Tacconi, L. J., Davies, R. I., et al., 2010, ApJ, 724, 233

Esquej, P., Alonso-Herrero, A., Pérez-García, A. M., et al., 2012, MNRAS, 423, 185

Farrah, D., Afonso, J., Efstathiou, A., et al., 2003, MNRAS, 343, 585

Fiore, F., Grazian, A., Santini, P., et al. 2008, ApJ, 672, 94

Franceschini, A., Braito, V., Persic, M., et al., 2003, MNRAS, 343, 1181

Frayer, D. T., Sanders, D. B., Surace, J. A., et al., 2009, AJ, 138, 1261

Gandhi, P., Horst, H., Smette, A., et al., 2009, A&A, 502, 457

Genzel, R., & Cesarsky, C. J. 2000, ARA&A, 38, 761

Genzel, R., Lutz, D., Sturm, E., et al. 1998, ApJ, 498, 579

Greve, T. R., Bertoldi, F., Smail, I., et al., 2005, MNRAS, 359, 1165

Haardt, F., & Maraschi, L., 1993, ApJ, 413, 507

Hopkins, P. F., Hernquist, L., Cox, T. J., & Kereš, D., 2008, ApJS, 175, 356

Hasinger, G., Cappelluti, N., Brunner, H., et al., 2007, ApJS, 172, 29

Ilbert, O., Arnouts, S., McCracken, H. J., Bolzonella, M., Bertin, E., et al., 2006, A&A, 457, 841

Ilbert, O., Capak, P., Salvato, M., et al., 2009, ApJ, 690, 1236

Imanishi, M., Maiolino, R., & Nakagawa, T., 2010, ApJ, 709, 801

Iono, D., Wilson, C. D., Takakuwa, S., et al., 2007, ApJ, 659, 283

Iwasawa, K., Sanders, D. B., Evans, A. S., et al., 2009, ApJ, 695, L103

Kartaltepe, J. S., Sanders, D. B., Le Floc'h, E., et al., 2010, ApJ, 709, 572

Kartaltepe, J. S., Dickinson, M., Alexander, D. M., et al., 2012, ApJ, 757, 23

Kocevski, D. D., Faber, S. M., Mozena, M., et al., 2012, ApJ, 744, 148

Koekemoer, A. M., Aussel, H., Calzetti, D., et al., 2007, ApJS, 172, 196

Komossa, S., Burwitz, V., Hasinger, G., et al., 2003, ApJ, 582, L15

Kormendy, J., & Richstone, D., 1995, ARA&A, 33, 581

Kovács, A., Chapman, S. C., Dowell, C. D., et al., 2006, ApJ, 650, 592

Lacy, M., Storrie-Lombardi, L. J., Sajina, A., et al., 2004, ApJS, 154, 166

Laird, E. S., Nandra, K., Pope, A., & Scott, D., 2010, MNRAS, 401, 2763

LaMassa, S. M., Heckman, T. M., Ptak, A., et al. 2012, ApJ, 758, 1

Lee, N., Le Floc'h, E., Sanders, D. B., et al., 2010, ApJ, 717, 175

Le Floc'h, E., Aussel, H., Ilbert, O., et al., 2009, ApJ, 703, 222

Lehmer, B. D., Alexander, D. M., Bauer, F. E., et al., 2010, ApJ, 724, 559

Levenson, N. A., Sirocky, M. M., Hao, L., et al., 2007, ApJ, 654, L45

Lilly, S. J., Le Fèvre, O., Renzini, A., et al., 2007, ApJS, 172, 70

Lilly, S. J., Le Brun, V., Maier, C., et al., 2009, ApJS, 184, 218

Lonsdale, C. J., Diamond, P. J., Thrall, H., Smith, H. E., & Lonsdale, C. J. 2006, ApJ, 647, 185

Lonsdale, C. J., Farrah, D., & Smith, H. E. 2006, Astrophysics Update 2, 285

Lutz, D., Maiolino, R., Spoon, H. W. W., & Moorwood, A. F. M. 2004, A&A, 418, 465

Magdis, G. E., Elbaz, D., Hwang, H. S., et al., 2010, MNRAS, 409, 22

Magdis, G. E., Daddi, E., Elbaz, D., et al., 2011, ApJ, 740, L15

Magnelli, B., Lutz, D., Santini, P., et al., 2012, A&A, 539, A155

Magorrian, J., Tremaine, S., Richstone, D., et al., 1998, AJ, 115, 2285

Mateos, S., Barcons, X., Carrera, F. J., et al. 2007, A&A, 473, 105

Mullaney, J. R., Alexander, D. M., Goulding, A. D., & Hickox, R. C., 2011, MNRAS, 414, 1082

Mullaney, J. R., Pannella, M., Daddi, E., et al., 2012, MNRAS, 419, 95

Netzer, H., Lutz, D., Schweitzer, M., et al., 2007, ApJ, 666, 806

Patel, H., Clements, D. L., Rowan-Robinson, M., & Vaccari, M., 2011, MNRAS, 415, 1738

Polletta, M., Tajer, M., Maraschi, L., et al., 2007, ApJ, 663, 81

Pozzi, F., Vignali, C., Gruppioni, C., et al., 2012, MNRAS, 423, 1909

Prescott, M. K. M., Impey, C. D., Cool, R. J., & Scoville, N. Z., 2006, ApJ, 644, 100

Press, W. H., Flannery, B. P., Teukolsky, S. A., & Vetterling, W. T., 1992, Numerical Recipes, 2nd edition (1992), Chapter 14

Ptak, A., Heckman, T., Levenson, N. A., Weaver, K., & Strickland, D., 2003, ApJ, 592, 782

Rafferty, D. A., Brandt, W. N., Alexander, D. M., et al., 2011, ApJ, 742, 3

Ranalli, P., Comastri, A., & Setti, G., 2003, A&A, 399, 39

Salvato, M., Hasinger, G., Ilbert, O., et al., 2009, ApJ, 690, 1250

Sanders, D. B., Soifer, B. T., Elias, J. H., et al., 1988, ApJ, 325, 74

Sanders, D. B., Soifer, B. T., Elias, J. H., Neugebauer, G., & Matthews, K., 1988, ApJ, 328, L35

Sanders, D. B., Phinney, E. S., Neugebauer, G., Soifer, B. T., & Matthews, K., 1989, ApJ, 347, 29

Sanders, D. B., & Mirabel, I. F., 1996, ARA&A, 34, 749

Sanders, D. B., Salvato, M., Aussel, H., et al., 2007, ApJS, 172, 86

Schawinski, K., Treister, E., Urry, C. M., et al. 2011, ApJL, 727, L31

Scoville, N., Aussel, H., Brusa, M., et al., 2007, ApJS, 172, 1

Scoville, N., Abraham, R. G., Aussel, H., et al., 2007, ApJS, 172, 38

Scott, K. S., Austermann, J. E., Perera, T. A., et al., 2008, MNRAS, 385, 2225

Shi, Y., Rieke, G., Lotz, J., & Perez-Gonzalez, P. G., 2009, ApJ, 697, 1764

Silverman, J. D., Lamareille, F., Maier, C., et al., 2009, ApJ, 696, 396

Smail, I., Swinbank, A. M., Ivison, R. J., & Ibar, E., 2011, MNRAS, 414, L95

Smith, B. J., Swartz, D. A., Miller, O., et al., 2012, AJ, 143, 144

Stansberry, J. A., Gordon, K. D., Bhattacharya, B., et al. 2007, PASP, 119, 1038

Stern, D., Eisenhardt, P., Gorjian, V., et al., 2005, ApJ, 631, 163

Symeonidis, M., Rosario, D., Georgakakis, A., et al., 2010, MNRAS, 403, 1474

Symeonidis, M., Georgakakis, A., Seymour, N., et al., 2011, MNRAS, 417, 2239

Tozzi, P., Gilli, R., Mainieri, V., et al., 2006, A&A, 451, 457

Treister, E., Cardamone, C. N., Schawinski, K., et al., 2009, ApJ, 706, 535

Treister, E., Natarajan, P., Sanders, D. B., et al., 2010, Science, 328, 600

Trichas, M., Georgakakis, A., Rowan-Robinson, M., et al., 2009, MNRAS, 399, 663

Trump, J. R., Impey, C. D., McCarthy, P. J., et al., 2007, ApJS, 172, 383

Tueller, J., Baumgartner, W. H., Markwardt, C. B., et al., 2010, ApJS, 186, 378

van der Werf, P. P., Isaak, K. G., Meijerink, R., et al., 2010, A&A, 518, L42

Veilleux, S. 2002, IAU Colloq. 184: AGN Surveys, 284, 111

Veilleux, S., Kim, D.-C., & Sanders, D. B., 2002, ApJS, 143, 315

Veilleux, S., Rupke, D. S. N., Kim, D.-C., et al., 2009, ApJS, 182, 62

Vignati, P., Molendi, S., Matt, G., et al. 1999, A&A, 349, L57

Voit, G. M., 1992, MNRAS, 258, 841

Walton, D. J., Roberts, T. P., Mateos, S., & Heard, V., 2011, MNRAS, 416, 1844

Wang, W.-H., Cowie, L. L., Barger, A. J., Keenan, R. C., & Ting, H.-C. 2010, ApJS, 187, 251

Yang, M., Greve, T. R., Dowell, C. D., & Borys, C., 2007, ApJ, 660, 1198

Yuan, T.-T., Kewley, L. J., & Sanders, D. B., 2010, ApJ, 709, 884
